# Maturation of persistent and hyperpolarization-activated inward currents shape the recruitment of motoneuron subtypes during postnatal development

**Simon A. Sharples and Gareth B. Miles**
School of Psychology and Neuroscience, University of St. Andrews, Fife, United Kingdom.

**Abstract:** The fine control of movement is a prerequisite for complex behaviour and is mediated by the orderly recruitment of motor units composed of slow and fast twitch muscle fibres. The size principle was initially proposed to account for orderly recruitment; however, motoneuron size is a poor predictor of recruitment amongst functionally defined motor unit subtypes. While intrinsic properties of motoneurons are key regulators of motoneuron recruitment, the underlying currents involved are not well defined. Whole-cell patch-clamp electrophysiology was deployed to study intrinsic properties, and the underlying currents, that contribute to the differential recruitment of fast and slow motoneurons. Motoneurons were studied during the first three postnatal weeks in mice to identify key properties that establish orderly recruitment and contribute to the emergence of fine motor control. We find that fast and slow motoneurons are functionally homogeneous during the first postnatal week and are recruited based on size, irrespective of motoneuron subtype. The recruitment of fast and slow motoneurons becomes staggered during the second postnatal week due to the differential maturation of passive and active properties, particularly persistent inward currents (PICs). The current required to recruit fast motoneurons increases further in the third postnatal week, despite no additional changes in passive properties or PICs. This further staggering of recruitment currents reflects development of a hyperpolarization-activated inward current during week 3. Our results suggest that motoneuron recruitment is multifactorial, with recruitment order established during postnatal development through the differential maturation of passive properties and sequential integration of persistent and hyperpolarization-activated inward currents.

**Key Points:**

- Fast and slow motoneurons become functionally diversified during postnatal development leading to the establishment of differential recruitment of fast and slow motoneuron subtypes.
- This functional development and diversification of motoneuron subtype recruitment is established through the differential maturation of passive and active properties.
- Fast motoneuron recruitment is delayed relative to slow motoneurons due to more depolarised thresholds for persistent inward currents and selective expression of a resting hyperpolarization-activated inward current.
- Recruitment of motoneuron subtypes is multifaceted and supported by differences in passive and active properties.

**Key words:** motoneuron, spinal cord, recruitment, size principle, intrinsic properties, postnatal development, electrophysiology

## Introduction

Fine control of muscle force is a prerequisite for the generation of complex movement. This fine control relies on the orderly recruitment of 'motor units'; the smallest functional unit of the motor system, consisting of alpha motoneurons and the muscle fibres they innervate [1]. Motor units can be subdivided based on the twitch kinetics of their muscle fibres. Different motor units are recruited in order of their force-generating capacity and susceptibility to fatigue, with slow fatigue resistant, fast fatigue resistant, and fast fatigable motor units recruited in sequence [2,3]. This orderly recruitment of motor units has been accounted for by the size principle [2–4], with smaller motor units recruited prior to larger motor units. Although motoneurons that make up different subtypes of motor units exist on a size-based continuum [5], there is considerable overlap in geometrical and physiological measures of size between motoneuron subtypes, such that motoneuron size appears to be a poor predictor of recruitment order [6,7]. It has therefore been argued that recruitment order is more heavily influenced by the functional subtype of a given motor unit and not strictly dependent on physical size [2,8–10]. Here we address whether motoneuron recruitment is purely dependent on the size principle, or whether functional classes of spinal motoneurons possess distinct electrophysiological properties that help ensure orderly recruitment of motoneuron subtypes.

The intrinsic excitability of neurons is influenced by their compartmental geometrical structures, which are endowed with specialized complements of ion channels that support flexible output [11–13]. For example, non-linearities in the input-output relationship of motoneurons are produced by persistent inward currents (PICs) generated by persistent sodium and L-type calcium channels located on the axon initial segment and distal dendrites respectively [14–22]. Variations in the complement of ion channels expressed by subtypes of spinal motoneurons have been demonstrated and their roles in producing non-linear firing behaviours described [11,23–25]. Many of these currents are activated below the spike threshold, meaning their differential expression is also likely to contribute to orderly recruitment across motoneuron subtypes [26].

To address the role of specific ion channels in motoneuron subtype recruitment, we studied differences in the intrinsic properties and underlying currents of fast and slow motoneurons by using whole-cell patch-clamp electrophysiological recordings in lumbar spinal cord slices of postnatal mice [24,27–30]. We used postnatal development as a model to dissect the relative importance of the intrinsic properties of motoneurons to the control of the orderly motoneuron recruitment required for fine motor control. Postnatal development in the rodent provides an opportune system to address this issue given that animals are largely sessile during the first postnatal week, produce rudimentary weight-bearing, hindlimb-based locomotion during week 2 [31], and complex locomotor behaviours consistent with adult animals by week 3 [32]. It would therefore be expected that key properties that establish orderly recruitment of functionally defined motoneuron subtypes would manifest in parallel with the emergence of complex motor behaviour during postnatal development.

We identify key properties and underlying currents of motoneuron subtypes and pinpoint when these properties contribute to the functional differentiation of motoneuron subtypes, particularly with respect to recruitment, during postnatal development. We find that during the first postnatal week, lumbar motoneurons are recruited according to passive properties predictive of size; however, fast and slow subtypes are functionally homogeneous leading to overlap in recruitment currents across motoneuron subtypes. Recruitment current of fast and slow motoneurons then becomes staggered by the second postnatal week due to both an increase in the size of fast motoneurons and delayed activation of sodium PICs in fast motoneurons. Recruitment current becomes staggered further during week 3, as fast motoneurons develop a hyperpolarization-activated inward current (Ih) that is active around resting

potential and delays recruitment by providing a depolarizing shunt. Taken together, our data demonstrate that motoneuron recruitment is multifactorial and support the notion that fast motoneurons are not simply scaled up versions of slow motoneurons [33]. Whilst recruitment is influenced by size, activation properties of inward currents, which are differentially expressed in motoneuron subtypes, ensure orderly recruitment of functionally defined subtypes of spinal motoneurons.

## Results

### Fast and slow motoneurons diversify functionally during postnatal development

We used whole cell patch clamp electrophysiology to define the intrinsic properties that differentiate motoneuron subtypes and support orderly recruitment. We adopted an established electrophysiological approach to identify fast and slow motoneurons in vitro based on their repetitive firing profiles in response to the injection of a 5 second depolarizing square current pulse at rheobase [24,27–30]. Fast motoneurons display a delayed repetitive firing profile with an accelerating firing rate (Figure 1B1), whereas slow motoneurons have an immediate repetitive firing profile with a steady or adapting firing rate (Figure 1B2). We identified delayed and immediate firing motoneurons at all ages studied (P1-20) with intrinsic properties that are consistent with those of fast and slow motoneurons (Figure 1C-E; Supplementary Table 1) [6,27,34,35]. Postnatal development in mice is highly stereotyped, with hindlimb weight-bearing emerging during the second postnatal week and complex locomotor behaviours emerging after the start of the third [32]. We therefore grouped motoneurons by week to explore broad changes in intrinsic properties of motoneuron subtypes between behaviourally defined milestones across motor development. Principle Component Analysis (PCA) was first deployed to identify global changes in intrinsic properties of motoneuron subtypes during development given the high dimensionality (25 variables) and large sample size (N = 261 motoneurons, 95 animals) of our data (Figure 2). This allowed us to focus subsequent analyses on variables that covary across motoneuron type during postnatal development.

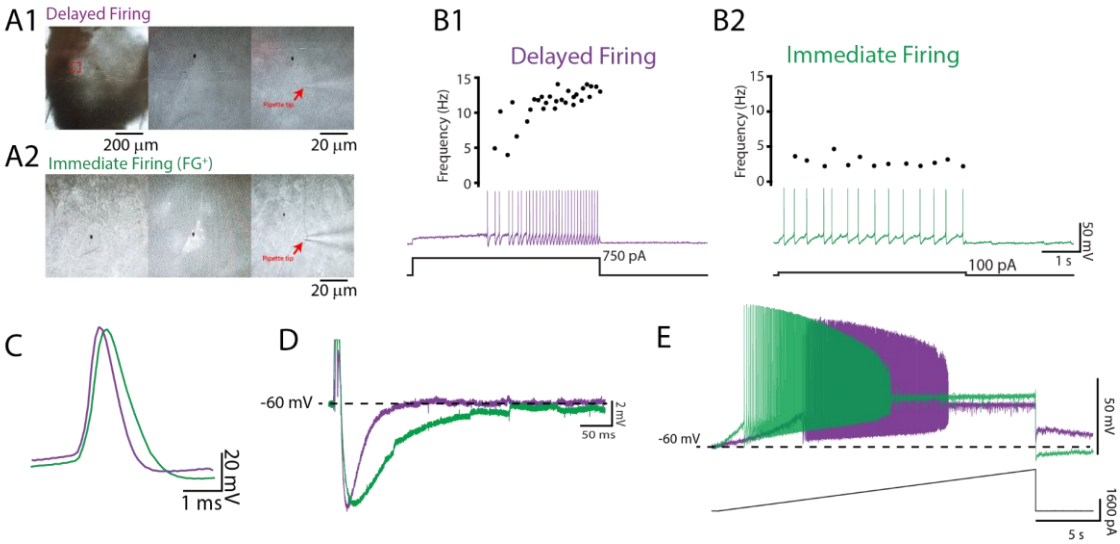


**Figure 1: Delayed and immediate firing motoneurons exhibit intrinsic properties consistent with fast and slow type motoneurons, respectively.** A.) Whole cell patch clamp recordings were obtained from motoneurons identified in the ventrolateral horn of the lumbar spinal cord with a subset retrogradely-labelled with fluorogold injected intraperitoneally. B1.) Fast type motoneurons (purple) were identified based on a delayed onset of repetitive firing and an accelerating firing rate during a 5 second depolarizing current step applied at rheobase. B2.) Slow type motoneurons (green) were identified based on an immediate onset for repetitive firing with a stable or adapting firing rate during a 5 second depolarizing current step applied at the rheobase. Single action potentials are broader (C), medium afterhyperpolarizations longer (D), and recruitment current lower (E) in immediate compared to delayed firing motoneurons.

PCA identified six principle components (PC's) that accounted for greater than 75% of variance; 48% of which was accounted for by PC1 and PC2 (Figure 2A). PC1 accounted for 35.54% of variance and as would be expected, had the greatest loading scores from recruitment current (0.82) and passive properties such as input resistance (-0.83) and membrane time constant (-0.7), but a relatively low weight from whole cell capacitance (0.54), which is related to cell surface area (Gustaffson and Pinter, 1984) (Figure 2B). Analysis of PC scores for PC1 revealed differential maturation in fast and slow motoneurons whereby PC1 scores increased in fast but did not change in slow motoneurons, with differences between fast and slow motoneurons revealed at weeks 2 and 3, but not week 1 (Figure 2D; $F_{(2,187)} = 14.1$, $p = 2.1e-6$). PC2 accounted for 14.02% of variance, had the greatest loading from action potential threshold voltage (0.77), which can also influence recruitment (Figure 2B), and matured in parallel in fast and slow motoneurons. PC2 scores were larger in slow motoneurons in week 1, decreasing in both subtypes, but to a greater extent in slow motoneurons, such that PC2 scores were more negative in slow compared to fast motoneurons in week 3 (Figure 2E; $F_{(2,228)} = 8.6$, $p = 2.5e-4$). PC3 accounted for 9.56% of variance and had the greatest loading score derived from repetitive firing properties such as maximum firing rate (0.78) and frequency-current gain within the sub-primary range (0.73) (Figure 2C). PC3 scores decreased in slow motoneurons only between weeks 2 and 3 (Figure 2F; $F_{(2.228)} = 21.9$, $p = 1.7e-9$). AHP half width is a strong predictor of motoneuron type [6] and in line with this, scored high for PC1 (-0.6) but relatively lower for PC2 (0.5) and PC3 (0.3). Further analysis revealed an increase in clustering of PCs 1-3 in fast and slow motoneurons as a function of development (Figure 2G-I) indicating that these two populations functionally diverge during postnatal development. PCs 4-6 accounted for less variance within our data (PC4: 7.4%; PC5: 5.5%; PC6: 4.8%) than PCs 1-3 and did not significantly change during development or reveal differences between motoneuron subtypes.

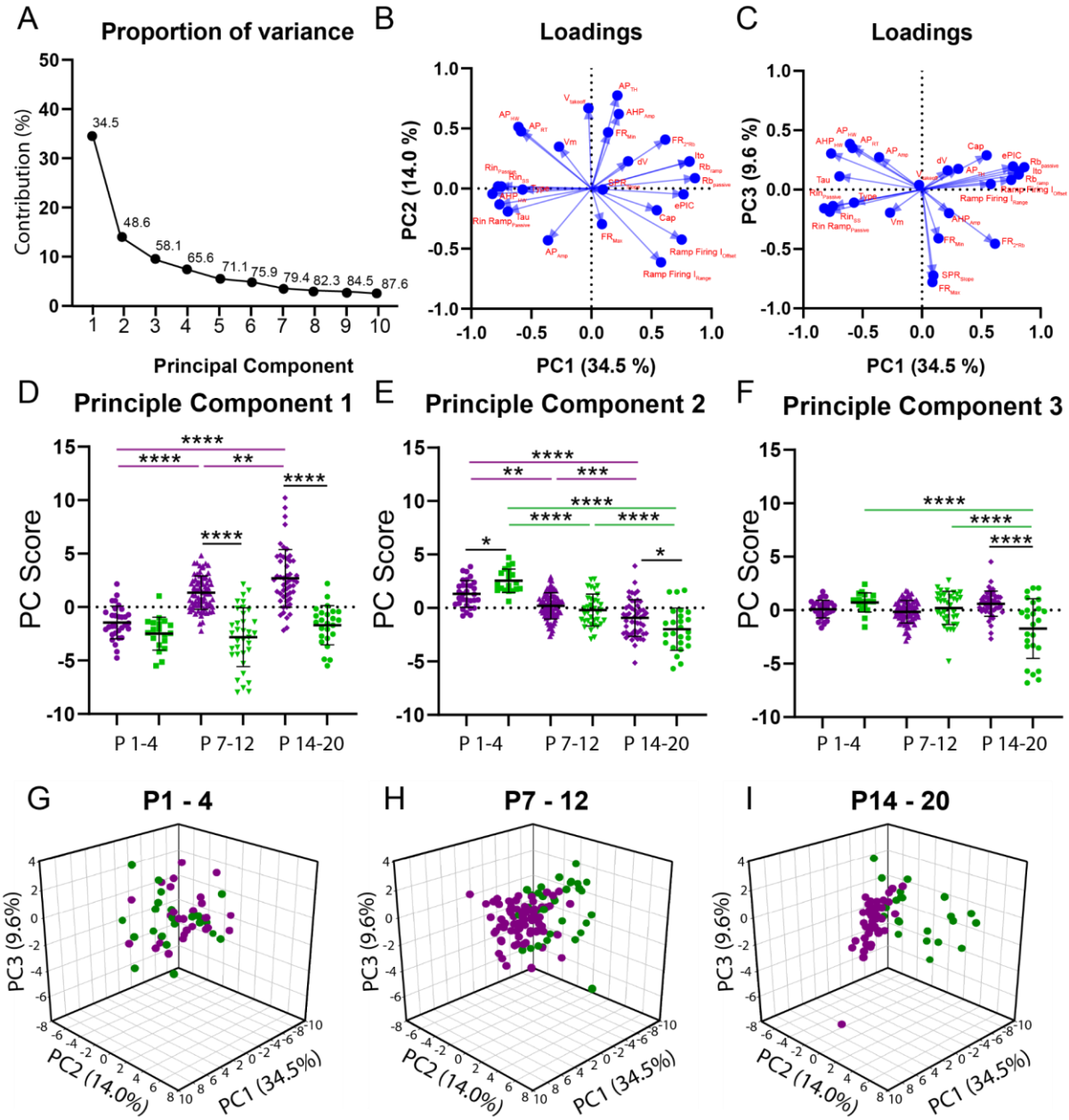


**Figure 2: Principle Component Analysis (PCA) reveals divergent maturation of the intrinsic properties of fast and slow motoneuron subtypes during postnatal development.** A.) Scree plot illustrating 10 Principle Components (PCs) identified in the PCA, with the first 6 accounting for greater than 75% of variance. B.) Variable loadings for PC1 and PC2 with arrow length representing loading score for each variable denoted in red text. C.) Variable loadings for PC1 and PC3 with arrow length representing loading score for each variable (red). D-F: PC scores for Principle Component 1-3 for fast (purple) and slow (green) type motoneurons across the first three weeks of postnatal development. Individual PC scores are displayed for each cell, black bars represent mean ± SD. Statistical analysis was conducted using a 2-way ANOVA and Holm-Sidak post hoc analysis. Asterisks denote significant differences from pairwise comparisons * $p < 0.05$, ** $p < 0.01$, *** $p < 0.001$, ****$p < 0.0001$. G-H: 3D scatterplots between PCs 1-3 for fast (purple) and slow (green) motoneurons across weeks 1-3.

**Postnatal diversification of intrinsic properties shapes the recruitment of motoneuron subtypes**
PCA indicated that recruitment current is a key predictor of the two motoneuron subtypes and can account for the greatest variance across postnatal development. We therefore next set out to determine intrinsic properties that mature in parallel, contribute to changes in recruitment during postnatal development, and would be likely to contribute to the establishment of orderly recruitment of motoneuron subtypes.

As would be expected based on the size principle, passive properties contributed substantially to the loading scores within PC1. Recruitment current and passive properties did not differ between fast and slow motoneurons during the first postnatal week (Figure 3D - G); however, recruitment current was correlated with passive properties such as capacitance and input resistance irrespective of motoneuron subtype at this point in time (Figure H1 - I1). This is supportive of an early recruitment scheme that is based on size rather than functionally defined subtypes of motoneurons.

Recruitment current then increased in fast but not slow motoneurons between weeks 1 and 2 (Figure 3D; $F_{(2,247)} = 12.1$, $p = 9.6e-6$). The non-uniform maturation of recruitment currents between motoneuron subtypes led to a 57% increase in the recruitment current range (W1: 909 pA; W2: 1596 pA) and a decrease in the recruitment gain across the samples of motoneurons studied (Figure 3E). In line with what would be predicted based on the size principle, we found a parallel increase in whole cell capacitance (Figure 3F; $F_{(2,253)} = 3.6$, $p = 0.03$) and a reduction in input resistance (Figure 3G; $F_{(2,253)} = 10.6$, $p = 3.9e-5$) in fast but not slow motoneurons between weeks 1 and 2. As a result, recruitment currents of fast and slow motoneurons become functionally staggered during week 2, whereby fast motoneurons have a significantly higher recruitment current, whole cell capacitance, and lower input resistance than slow type motoneurons. The membrane time constant increased between weeks 1 and 2 in slow but not fast motoneurons, leading to a longer time constant in slow compared to fast motoneurons during week 2 (Supplementary Table 1; $F_{(2,253)} = 7.9$ $p = 4.7e-4$). Together these results indicate that maturation of motoneuron passive properties contribute to the functional specification of motoneuron subtypes during the second postnatal week.

Recruitment current increased further in fast but not slow motoneurons between weeks 2 and 3 (Figure 3D; $F_{(2,247)} = 12.1$, $p = 9.6e-6$), leading to a 182% increase in recruitment range compared to week 2 and a 320% increase compared to week 1 (W3: 2906 pA) and a further decrease in the recruitment gain (Figure 3E). However, the increase in recruitment current in week 3 was not paralleled by further changes in passive properties. In fact, the relationship between recruitment current and capacitance appears to become weaker over this time period (Figure 3H: W1: $r^2 = 0.35$, W2: $r^2 = 0.27$, W3: $r^2 = 0.25$). This result suggests that recruitment, and its maturation between weeks 2 and 3, may not be solely dependent on passive properties, as would be predicted by the size principle.

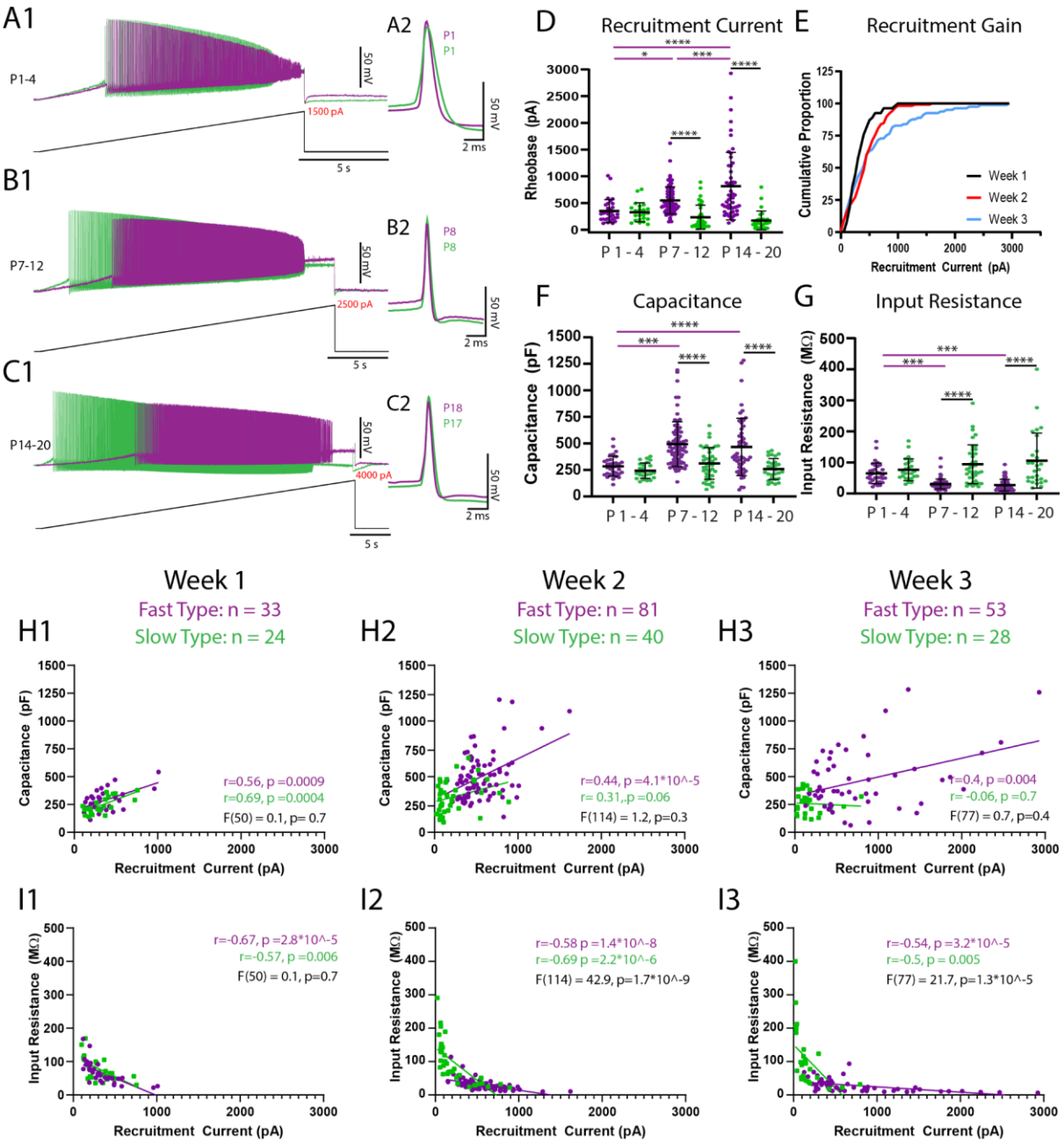


**Figure 3: Passive properties contribute to maturation of recruitment between weeks 1 and 2 but additional factors contribute from weeks 2 to 3.** Recruitment of fast (purple) and slow (green) type motoneurons was assessed using slow (100pA/s) depolarizing current ramps. A-C: Representative traces of recruitment and repetitive firing of fast and slow motoneurons at weeks 1-3. A2-C2: First action potential produced upon recruitment for fast and slow motoneurons at weeks 1-3. D.) Recruitment current (rheobase) increases in fast but not slow motoneurons across weeks 1-3. E.) Cumulative proportion histograms of recruitment currents of motoneurons sampled during weeks 1 (black), 2 (red), and 3 (blue) indicate a progressive decrease in the recruitment gain. F.) Whole cell capacitance increases and input resistance decreases (G) in fast but not slow motoneurons between weeks 1 and 2 but not further into week 3. Individual data points are displayed, black bars represent mean ± SD. Statistical analysis was conducted using a 2-way ANOVA and Holm-Sidak post hoc analysis. Asterisks denote significant differences from pairwise comparisons * $p < 0.05$, ** $p < 0.01$, *** $p < 0.001$, ****$p < 0.0001$. Scatterplots of recruitment current, and passive properties (H: Whole cell capacitance; I: Input resistance) [6], for fast ( purple) and slow (green) motoneurons during postnatal weeks 1, 2 and 3. Pearson correlations were performed for each type at each time point with outcomes displayed in purple text for fast and green text for slow type motoneurons. A simple linear regression comparing the regression slopes for each motoneuron subtype at each time point was performed to determine the degree of similarities between subtypes with outcomes displayed in black text.

**Persistent inward currents contribute to the recruitment of fast and slow motoneurons**

Changes in the membrane potential of motoneurons in response to slow depolarizing current ramps are characterized by two phases: an initial linear phase, presumably predominated by passive properties, and an accelerating depolarization of the membrane potential (Figure 4A), mediated by the activation of persistent inward currents (PICs) [36–38]. We find evidence for both phases in fast and slow motoneurons at all ages (P1 - 20). PICs have been extensively studied in spinal motoneurons and underlie non-linear firing behaviours [14,22,23], but their relative contribution to recruitment have been less explored. We therefore next tested the possibility that PICs may have a larger impact on the trajectory of the membrane potential in slow motoneurons compared to that of fast motoneurons and may therefore shape their recruitment at stages when our data suggest that differential recruitment cannot be governed by size-based principles alone.

The influence of PICs on recruitment were first estimated by calculating the difference between the measured recruitment current and an estimate of what the recruitment current would be if the membrane depolarisation followed a linear trajectory determined by passive properties alone (Fig. 4A $I_{passive}$ - $I_{actual}$; ePIC) [38,39]. ePIC did not differ between fast and slow motoneurons in week 1, increased in fast motoneurons only in weeks 2 and 3, and was larger in fast compared to slow motoneurons at both time points (Figure 4B: $F_{(2,242)} = 10.2$, $p = 5.7e-5$). We also assessed the influence of PICs on motoneuron output during triangular depolarizing current ramps as an additional and well-established estimate of PIC magnitude [16,20,22,40]. In this assay, a lower current at derecruitment on the descending limb of the triangular ramp compared to the recruitment current on the ascending limb (negative Delta I) is evidence of a PIC. Delta I did not differ between fast and slow motoneurons during week 1, became more negative (increased PIC) in fast motoneurons during week 2, but did not change further into week 3 (Supplemental Figure 1; $F_{(2,165)} = 6.1$, $p = 0.003$).

The underlying PICs were next measured directly in voltage clamp during slow (10 mV/s) depolarizing voltage ramps (Figure 4E) [17,20] to account for the possibility that current clamp-based estimates of PIC may not be purely dependent on PICs. In line with our two estimates of PICs measured in current clamp, the amplitude of the PIC measured in voltage clamp was significantly larger in fast compared to slow motoneurons at weeks 2 and 3 (Figure 4F; $F_{(1,61)} = 17.9$, $p = 7.8e-5$), which can be accounted for by the larger size (higher capacitance) of fast compared to slow motoneurons given that PIC density (current/whole cell capacitance) did not differ between subtypes (Supplementary Table 2). PIC amplitude did not change in either subtype between weeks 2 and 3 (Figure 4G; $F_{(1,61)} = 0.02$, $p = 0.9$) and was not correlated with recruitment current at either age (W2: $r = -0.1$, $p = 0.5$; W3: $r = -0.2$, $p = 0.2$).

Differences in the magnitude of PICs between fast and slow motoneurons do not appear to explain differential recruitment or motoneuron subtypes or changes that we observe during development; in fact, they might support earlier recruitment in fast motoneurons. We therefore considered other factors, which may contribute to differential recruitment, such as the voltage at which PICs first activate. We found no difference in the voltage at which depolarisation of the membrane potential began to accelerate, in response to slow depolarising current ramps, between fast and slow motoneurons during week 1. However, the onset of the acceleration phase became hyperpolarized in both fast and slow motoneurons in week 2 and continued to hyperpolarize even further in the slow motoneurons into week 3, becoming significantly more hyperpolarized compared to fast motoneurons (Figure 4C; $F_{(2,247)} = 6.1$, $p = 0.003$). Interestingly, acceleration onset voltage and spike threshold matured in parallel (Figure 5D), such that the amplitude of the depolarizing acceleration from onset to spike threshold, were similar between fast and slow motoneurons and maintained at all ages (Supplementary Table 2; $F_{2,247)} = 2.2$, p

= 0.1). In line with estimates of PICs in current clamp, PIC onset voltage measured in voltage clamp was more depolarized in fast compared to slow motoneurons at both weeks 2 and 3 ($F_{1,61}$ = 57.6, p = 2.2e-10), did not change between weeks 2 and 3 in either motoneuron type (Figure 4G; $F_{(1,61)}$ = 0.2, p = 0.7), but was correlated with recruitment current at both ages (W2: r = 0.4, p = 0.007; W3: r = 0.7, p = 1.3e-5). Interestingly, PIC activation in slow motoneurons occurs relatively close to their respective resting membrane potential (RMP: W2: -58.3 ± 5.4; W3: -61.5 ± 6.7 mV) which may facilitate their recruitment (Supplementary Table 1; Supplementary Table 2).

PICs are produced by a combination of ion channels that conduct sodium and calcium currents, with sodium PICs activated at more hyperpolarized voltages than calcium PICs [18,20]. To determine the relative importance of each type of PIC to recruitment of fast motoneurons, we deployed pharmacological tools to block NaV1.6 channels [18,21,41,42] and L-type calcium channels (ICaL: [15,43–47], which conduct sodium and calcium PICs respectively. Blocking either NaV1.6 channels with the selective blocker, 4,9-Anhydrotetrodotoxin (4,9-AH-TTX: 200 nM; n = 22 MNs, 11 animals) or L-type calcium channels with nifedipine (20 µM; n = 16 MNs, 9 animals) reduced PIC amplitude (Figure 4I: 4,9-AH-TTX: 31% reduction; $t_{(19)}$ = 3.8, p = 0.001; Nifedipine: 22% reduction; $t_{(14)}$ = 2.6, p = 0.02). However, only blocking NaV1.6 channels depolarized the PIC onset voltage (Figure 4J; 4,9-AH-TTX: $t_{(19)}$ = 4.2, p = 5.1e-4; Nifedipine: $t_{(14)}$ = 1.2, p = 0.3). Blocking NaV1.6 or L-Type calcium channels increased input resistance (Figure 4L: 4,9-AH-TTX: $t_{(19)}$ = 2.4, p = 0.03; Nifedipine: $t_{(14)}$ = 3.2, p = 0.007). However, only blocking NaV1.6 channels translated to an increase in recruitment current (Figure 4M: $t_{(19)}$ = 9.7, p = 1.5e-8) which decreased the recruitment gain (Figure N), whereas blocking the L-type calcium channels did not significantly change the recruitment current (Figure 4M: $t_{(14)}$ = 1.6, p = 0.12) or gain (Figure 4O).

These data indicate that PIC activation threshold, which is regulated by sodium PICs, is more important for shaping recruitment than the overall PIC amplitude, which is generated by a combination of sodium and calcium currents. Further, recruitment current is not purely dependent on input resistance and is also influenced by properties of currents that are activated in the subthreshold voltage range. Thus, in addition to passive properties, maturation of PICs appears to contribute to the emergence of orderly recruitment amongst motoneuron subtypes in week 2. However, it is unlikely that PICs contribute to further increases in the recruitment current of fast motoneurons into week 3, given that PIC onset voltage, which is the most important property of the PIC for recruitment, does not change between weeks 2 and 3.

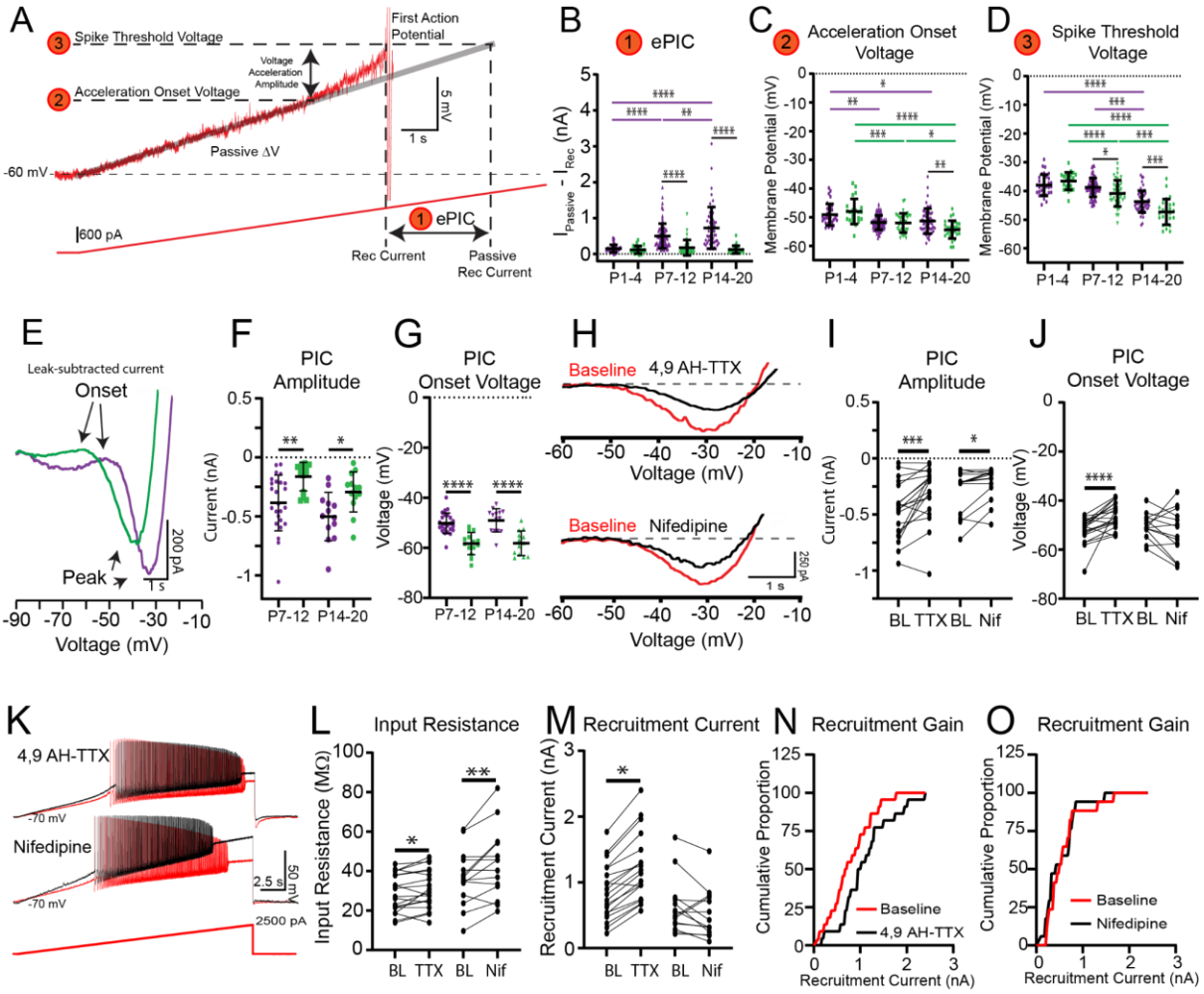


**Figure 4: PIC maturation shapes motoneuron recruitment.** A.) Recruitment was assessed using a slow depolarizing current ramp (100 pA/s from -60 mV). During these ramps, the trajectory of the membrane potential approaching the spike threshold is characterised by a passive, linear phase (DV: grey line) and an accelerating phase. The impact of the underlying current producing the membrane potential acceleration, termed ePIC (A1, B), is estimated as the difference between the extrapolated passive and actual recruitment currents. The acceleration onset voltage (A2, C) is the voltage at which the membrane potential deviates by greater than 1 mV from the linear function fitted to the initial (passive) depolarization of the membrane potential during the ramp. The amplitude of this acceleration phase is calculated from the onset voltage to the threshold of the first action potential (A3, D). E.) Persistent inward currents (PICs) were measured in voltage clamp from fast and slow motoneurons of 2-week (n = 25 fast; n = 14 slow) and 3-week (n = 14 fast; n = 13 slow) old mice using a slow depolarizing voltage ramp (10mV/s; -90 to -10 mV). PIC onset and amplitude were measured from leak-subtracted, low pass filtered (5Hz Bessel) traces. F.) PICs were larger in amplitude in fast compared to slow motoneurons at both 2 and 3 weeks. G.) PIC onset was significantly more depolarized in fast compared to slow motoneurons and did not change between weeks 2 and 3. Statistical analysis was conducted using a 2-way ANOVA and Holm-Sidak post hoc analysis. H.) The relative contribution of NaV1.6 and L-type calcium channels to PICs in fast motoneurons was tested with 4,9-Anhydrotetrodotoxin (4,9 AH-TTX; 200 nM, n = 22) and nifedipine (20 μM, n = 16) respectively (black traces). Both 4,9 AH-TTX and nifedipine significantly reduced PIC amplitude (I); only 4,9 AH-TTX depolarized PIC onset voltage (J). K.) Representative traces from depolarizing current ramps used to investigate recruitment before (red) and after (black) blocking NaV1.6 or L-type calcium channels. L.) Blocking either Nav1.6 or L-type calcium channels increased input resistance, however only blocking NaV1.6 channels led to an increase in recruitment current (M). Individual data points are displayed, black bars represent mean ± SD. Statistical analysis was conducted using a 2-way ANOVA (B-G, J-K) and Holm-Sidak post hoc analysis or paired t-tests. Asterisks denote significant differences from pairwise comparisons * $p < 0.05$, ** $p < 0.01$, *** $p < 0.001$, **** $p < 0.0001$. Cumulative proportion histograms for recruitment currents of fast motoneurons sampled before (red) and after (black) blocking NaV1.6 channels (N) or L-type calcium channels (O).

**Hyperpolarization-activated inward currents shape the recruitment of fast and slow motoneurons after week 3**

We next considered other active properties that might contribute to the increase in recruitment current in fast motoneurons between weeks 2 and 3 and further stagger recruitment of fast and slow motoneuron subtypes. HCN channels produce a hyperpolarization-activated inward current (Ih) and are key for producing rebound bursting following inhibition [48–51]. In some neurons, HCN channels are active near resting potential, producing an inward current that counteracts the hyperpolarizing influence of a potassium leak current to maintain the resting membrane potential [52–56]. Putative Ih-mediated sag potentials have been described in larger spinal motoneurons of adult cats and rats [6,7,39,57–62], and have been suggested to decrease the mAHP; a key distinguishing feature of motoneuron subtypes. We therefore hypothesized that an increase in Ih in fast but not slow motoneurons during week 3 may become important for shaping fast motoneuron recruitment and therefore further refining orderly recruitment.

In line with our hypothesis, we found a prominent increase in depolarizing sag potentials measured in current clamp (Figure 5A-D) and underlying Ih measured in voltage clamp (Figure 5E-I) in fast motoneurons at week 3, which was abolished by the selective HCN channel blocker, ZD-7288 (10 µM: Figure 5J-O) (Fast: Figure 5J, L: $F_{(1,11)} = 15.7$, $p = 0.003$; Slow: Figure 6N: $F_{(1,9)} = 19.6$, $p = 0.004$). The overall sag conductance was estimated (gSag) by calculating the inverse of the I-dV slope (conductance: g) at initial and steady state potentials during hyperpolarizing current steps and then compared between motoneuron subtypes across development. gSag did not differ between fast and slow motoneurons during weeks 1 and 2 but increased in fast motoneurons at week 3 such that it was larger in fast compared to slow motoneurons at this point in time (Figure 5B; $F_{(2,249)} = 5.2$, $p = 0.006$). Depolarizing sag potentials (Figure 5C; $F_{(6,103)} = 28.4$, $p < 1.0e-15$) and underlying Ih amplitude (Figure 5G; $F_{(4,142)} = 33.0$, $p < 1.0e-15$) were larger in fast compared to slow motoneurons during week 3. Notably, we find a prominent Ih in fast motoneurons at -70 mV (Supplementary Table 2), which is near the resting potential of fast motoneurons (Ih -70 mV W3: -119 ± 103 pA; RMP W3: -66.8 ± 3.6 mV). Ih density was larger in fast compared to slow motoneurons at week 3 (Figure 5I; $F_{(4,142)} = 6.5$, $p = 7.7e-5$), but not week 2 (Figure 5H; $F_{(4,100)} = 0.3$, $p = 0.9$), suggesting that differences in Ih at week 3 are not due to differences in soma size.

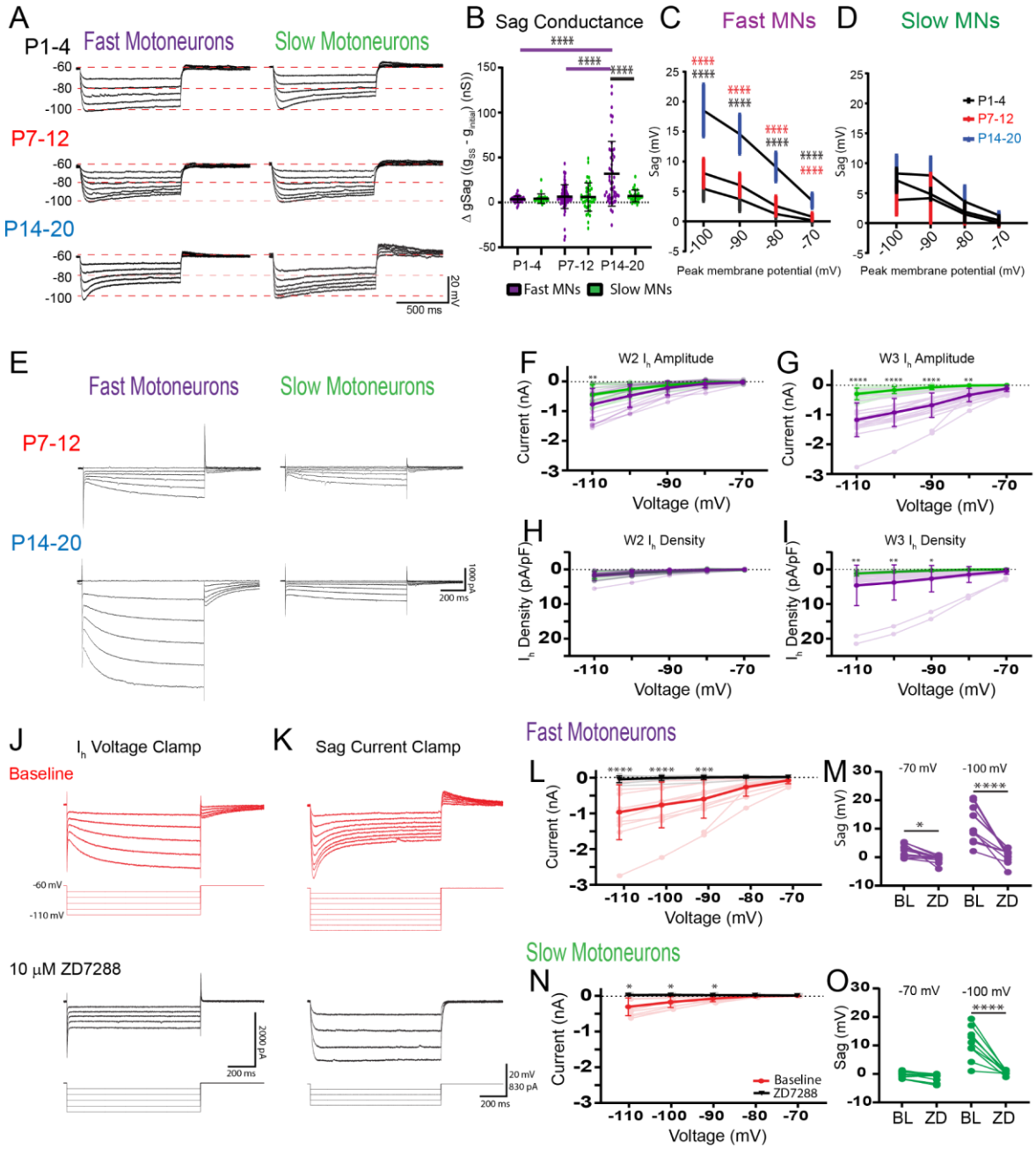


**Figure 5: Fast motoneurons develop a resting Ih in week 3.** A.) Sag potentials were measured from fast (purple) and slow (green) motoneurons of mice aged P1-4 (n = 54), P7-12 (n = 122), and P14-20 (n = 81). B.) The sag conductance (gSag) was estimated (eSag Conductance) during a series of hyperpolarizing current steps (1 s duration). Sag potentials plotted as a function of trough of membrane potential for fast (C.) and slow (D) motoneurons at P1-4 (black), P7-12 (red), and P14-20 (blue). E.) Ih was measured in fast and slow motoneurons during weeks 2 (fast: n= 15; slow: n= 12) and 3 (fast: n = 19; slow: n = 19) in voltage clamp using a series of incremental hyperpolarizing voltage steps (-60 to -110 mV, 1 s duration, 10 mV increments). Ih in fast (purple) and slow (green) motoneurons at week 2 (F) and week 3 (G) plotted as a function of voltage. Ih density of fast and slow motoneurons at week 2 (H) and 3 (I). Representative trace of Ih recorded in voltage clamp (J) and depolarizing sag potential recorded in current clamp (K) from a fast type motoneuron before (red trace) and after (black trace) bath application of the HCN channel blocker ZD7288 (10 μM). L.) Ih IV plots from fast (n = 13) motoneurons before (red) and after (black) ZD7288. M.) ZD 7288 significantly reduced depolarizing sag potentials measured in fast motoneurons at a peak voltage of -70 mV and -100 mV. N.) Ih IV plots from slow motoneurons (n = 9) before (black) and after (red) ZD7288. O.) ZD 7288 significantly reduced depolarizing sag potentials measured in slow motoneurons at a peak voltage of -100 mV but not -70 mV. Data are presented as individual points for each cell studied. Statistical analyses were conducted using 2-way ANOVA and Holm-Sidak post hoc analysis when significant effects were detected. Asterisks denote significant differences from Holm-Sidak post hoc analysis * $p < 0.05$, ** $p < 0.01$, *** $p < 0.001$, **** $p < 0.0001$.

We next tested the hypothesis that Ih delays the recruitment of fast motoneurons by acting as a slowly inactivating depolarizing leak current. For Ih to influence recruitment, it would need to be active at resting membrane potential. Ih is an inward current, therefore it would be expected that cells with an active Ih at rest would have a more depolarized resting membrane potential and smaller mAHP. Consistent with this notion, Ih amplitude measured near resting membrane potential, during a hyperpolarizing voltage step from -60 mV to -70 mV, was larger in cells that had a more depolarized resting membrane potential (Figure 6B: $r = -0.6$, $p = 0.002$). Blocking Ih with ZD-7288 hyperpolarized the resting membrane potential of both fast and slow motoneurons (Figure 6C: $F_{(1,20)} = 11.0$, $p = 0.003$), however the magnitude of this change was greater in fast motoneurons (Figure 6D: $t_{(20)} = 3.3$, $p = 0.003$). Ih measured at -70 mV was also larger in cells with a smaller mAHP amplitude (Figure 6F: $r = -0.73$, $p = 3.1e-4$; Ih density: $r = -0.73$, $p = 2.0e-4$) and blocking Ih with ZD-7288 increased the amplitude of the mAHP in fast but not slow motoneurons (Figure 6G: $F_{1,16)} = 5.3$, $p = 0.03$), suggesting that Ih is active at resting membrane potential and may therefore influence recruitment.

Ih measured at -70 mV was larger in motoneurons with a higher recruitment current (Figure 6J: $r = -0.86$, $p = 6.4e-7$) and ZD-7288 decreased the recruitment current of fast but not slow motoneurons (Figure 6K: $F_{(1,20)} = 5.4$, $p = 0.0002$), to a level where recruitment current of fast motoneurons was not significantly different from that of slow motoneurons at their respective baseline (Figure 6KR: Holm-sidak post hoc: $p = 0.19$). This non-uniform modulation of recruitment currents across motoneuron subtypes led to a 50% reduction in the recruitment current range across the sample of motoneurons studied (BL: 3227 pA; ZD7288: 1624 pA) and an increase in the recruitment gain (Figure 6L). ZD-7288 did not change the voltage threshold of the first action potential in either motoneuron type (Fast: BL: -38.8 ± 3.9, ZD: -37.8 ± 7.4 mV; Slow: -45.0 ± 4.1, ZD: -45.2 ±3.4 mV; $F_{(1,20)} = 0.6$, $p = 0.5$).

Together these results indicate that 1.) fast motoneurons express an active Ih at resting potential which shapes both the mAHP and recruitment current, likely by acting as a depolarizing leak current and 2.) differential maturation of Ih in fast versus slow motoneurons is likely to underlie the further refinement of recruitment order and expansion of the recruitment range from postnatal weeks 2 to 3.

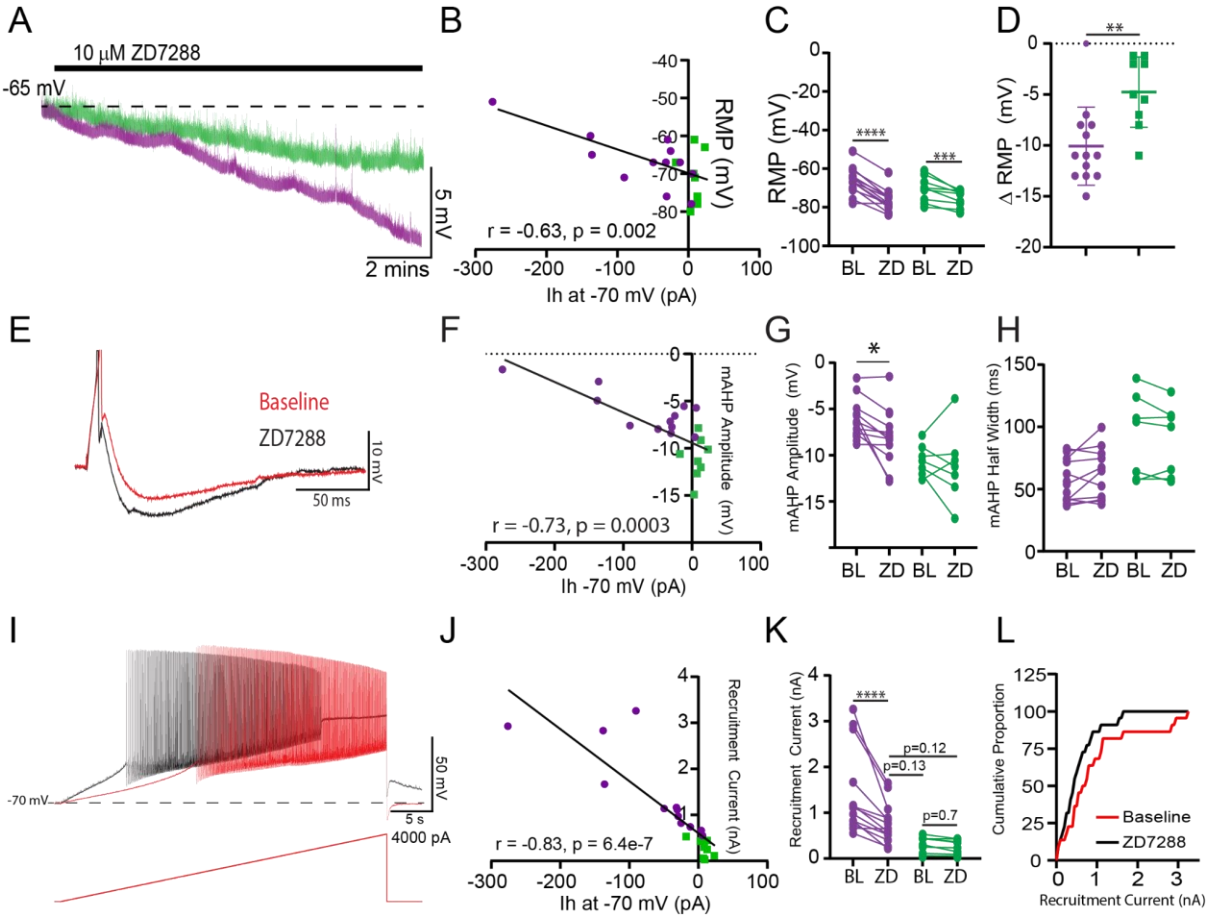


**Figure 6: A resting Ih decreases the mAHP and increases recruitment current of fast motoneurons at week 3.** A.) Representative traces of the resting membrane potential (RMP) of fast (purple: n = 13)) and slow (green: n = 9) motoneurons from lumbar slices of P14-20 mice during blockade of HCN channels with ZD7299 (10 µM). B.) RMP was correlated with Ih measured at -70 mV in voltage clamp at baseline (Pearson Correlation). C.) ZD7288 hyperpolarized the RMP of both fast and slow motoneurons; however, the magnitude of the hyperpolarization was larger in fast motoneurons (D: unpaired t-test). E.) Representative trace of the medium afterhyperpolarization (mAHP) elicited by a 10 ms depolarizing current step before (red) and after (black) blockade of HCN channels. F.) mAHP amplitude was correlated with Ih measured at -70 mV in voltage clamp at baseline (Pearson Correlation). G.) ZD7288 increased the amplitude but not the half width (H) of the mAHP. I.) Representative voltage trace of a fast type motoneuron during a slow depolarizing (100 pA/s) recruitment ramp before (red) and after (black) ZD7288. J.) Recruitment current was correlated with Ih measured at -70 mV in voltage clamp at baseline (Pearson Correlation). K.) ZD7288 reduced the recruitment current of fast (purple) but not slow motoneurons. Data are presented as individual points for each cell studied. Statistical analyses were conducted using 2-way ANOVA and Holm-Sidak post hoc analysis when significant effects were detected. Asterisks denote significant differences from Holm-Sidak post hoc analysis * $p < 0.05$, ** $p < 0.01$, *** $p < 0.001$, **** $p < 0.0001$. L.) Recruitment gain represented by cumulative proportion histograms of recruitment currents of motoneurons sampled before (red) and after (black) blocking HCN channels.

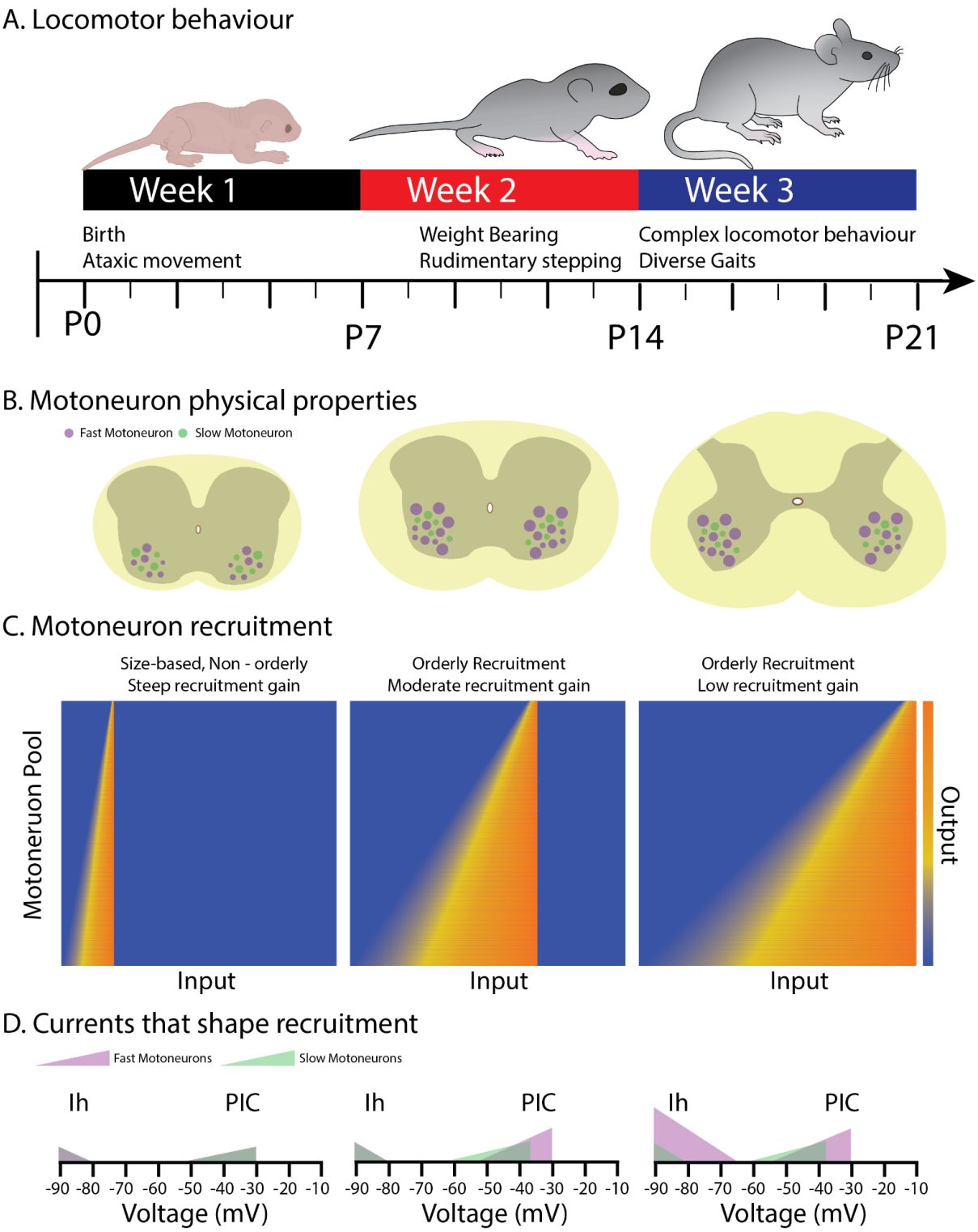


**Figure 7:** Schematic summarizing changes in the physical properties, recruitment, and underlying currents in motoneuron subtypes that shape the orderly recruitment and recruitment gain of motoneurons during postnatal development as complex locomotor behaviours emerge. Fast motoneurons and their underlying currents are depicted in purple and slow motoneurons, and their underlying currents depicted in green.

**Discussion**

We set out to address whether motoneuron recruitment is purely dependent on the size principle, or whether functional classes of spinal motoneurons possess distinct electrophysiological properties that help ensure orderly recruitment of motoneuron subtypes. We used postnatal development of the mouse as a model to dissect the relative importance of motoneuron intrinsic properties to the establishment of orderly recruitment during the emergence of fine motor control. The rate at which motoneurons within a motor pool are recruited is important because it defines the recruitment gain and influences the relative degree of precision or vigour of movement [10,63,64]. We reveal novel roles for specific ion channels in shaping motoneuron subtype recruitment and demonstrate sequential integration of these intrinsic properties during postnatal development. These findings are of broad importance given that orderly recruitment of motoneurons is conserved across phyla [2,3,6,27,28,34,35,61,65–70], and differences in the intrinsic properties of motoneuron subtypes lead to increased susceptibility to degeneration in disease [27,35,71–73] subsequently producing motor dysfunction as a consequence of alterations in recruitment gain within motor pools [74–76].

Our results suggest that motoneuron recruitment is multifaceted, with multiple layers that establish orderly recruitment of functionally defined spinal motoneuron subtypes. The size principle forms a foundation with recruitment directed by physical properties of neurons. We find that during the first postnatal week recruitment is driven primarily by the physical properties of neurons, as would be predicted by the size principle, but recruitment is not linked to the functional subtypes of motoneurons. A steep recruitment gain within a motor pool, with no differentiation between the recruitment of motoneuron subtypes, may be important to facilitate the rapid, ballistic movements, which are typically observed in new-born mice prior to the onset of finer motor control. These findings are consistent with those in human babies where rapid movements are supported by synchronized recruitment of motor unit subtypes to accommodate for the slower and more homogenous muscle twitch properties at early postnatal stages [77], which have also been reported in neonatal rodents [78]. Synchronized motoneuron recruitment may also support ongoing maturation of spinal circuits and neuromuscular junctions during early postnatal development [79] when poly-neuronal innervation of muscle fibres [80,81], in addition to gap junction [82–84] and glutamatergic coupling [30] between motoneurons remains prevalent.

Recruitment of fast and slow motoneurons becomes staggered during the second postnatal week, when finer motor control develops, such as hindlimb weight-bearing during stepping. This separation of recruitment coincided with the diversification of motoneuron subtypes as revealed by our principle component analysis and supported by previous work [85]. A portion of this staggered recruitment relates to differential maturation of passive properties, with fast motoneurons increasing in size, as indexed by whole cell capacitance, leading to a decrease in input resistance. This is in line with previous reports demonstrating increases in motoneuron size during the first two postnatal weeks [86–88]. However, previous work in adult cat motoneurons, suggests that variation in cell size or input resistance cannot account for the full range of recruitment currents across a motor pool [89]. In addition to passive properties related to size, we found that active properties, determined by specific ion channels, differed between motoneuron subtypes, and changed during development. This suggested that changes in active properties contribute to the separation of motoneuron subtype recruitment from the second postnatal week onwards. These active properties produce non-linearities in the input-output functions of motoneurons, based on distinct activation and inactivation properties of voltage-sensitive ion channels. The developmental emergence of a role for active properties in motoneuron recruitment may provide more flexible motor output than would be possible if recruitment was based on a fixed set of physical parameters such as motoneuron size. This may be critical for fine motor control as more complex motor behaviours emerge.

We first found that persistent inward currents (PICs) contribute to motoneuron recruitment from the second postnatal week. PICs are well described in motoneurons [14,16,18,20,22,23,90] where they amplify synaptic inputs to distal dendrites [13,91,92] and are critical for the generation of repetitive firing [36,47,93]. In some cases, PICs also produce plateau potentials and lead to bistability, which can sustain repetitive firing following the termination of excitatory synaptic input [17]. We expected to find larger PICs in slow motoneurons given their lower recruitment currents and greater tendency for bistability [94], which is thought to be important for the maintenance of posture. However, we found that PIC amplitude was larger in fast compared to slow motoneurons, although when correcting for cell size we found no difference in PIC density between subtypes. Further analyses revealed a difference in the activation voltages of PICs across motoneuron subtypes, with PICs activating at more depolarised potentials in fast motoneurons. These data demonstrate that variations in the activation voltage of PICs help drive differential recruitment across motoneuron subtypes.

PICs are produced by a complement of ion channels that conduct sodium and calcium currents. Our pharmacological analysis demonstrated that NaV1.6 channels and L-type calcium channels contribute to PICs in fast motoneurons. Although it is important to note that other ion channels likely contribute to motoneuron PICs [47] given that blockade of Nav1.6 and L-type calcium channels only produced a 48 % reduction in PIC amplitude. We found that NaV1.6, rather than L-type calcium channels, determines the PIC activation voltage, and shapes recruitment by controlling the voltage trajectory approaching the spike threshold. This is in line with previous experimental [36] and computational work [26]. NaV1.6 channels are well-placed to control recruitment, given their dense expression at the axon initial segment (AIS) [21,39], a specialized structure that is critical for the generation of action potentials and support of repetitive firing. Other channels, including KV1.2 channels, which underlie the characteristic delayed firing behaviour of fast motoneurons [24,27,28], are also clustered at the AIS and may dynamically interact with NaV1.6 channels to shape recruitment current. Furthermore, given that the AIS is further from the soma in fast compared to slow motoneurons [95], physical properties of the AIS may also contribute to differential recruitment of motoneuron subtypes. If so, one might predict that the distance between soma and AIS may increase in fast motoneurons during the first two postnatal weeks and contribute to functional specification of motoneuron subtypes.

We found that recruitment current of fast motoneurons increased further from the third postnatal week, paralleling the emergence of more complex locomotor behaviours, similar to those seen in adults [32]. However, this increase in fast motoneuron recruitment current could not be accounted for by changes in passive properties or PICs. Instead, we found that a hyperpolarization-activated inward current (Ih) mediated this further refinement of fast motoneuron recruitment. Ih is a non-specific inward current conducted by HCN channels, which are located on the somata and proximal dendrites of larger motoneurons in the rodent spinal cord [96]. Although depolarizing sag potentials [6,38,54,58,61,62] and developmental changes in Ih have been reported previously in motoneurons [53,97,98], the functional significance of these findings was unclear. We found a prominent increase in Ih density, measured at voltages near resting membrane potential, in fast but not slow motoneurons at week 3. Blocking HCN channels with ZD7288, led to a decrease in recruitment current of fast but not slow motoneurons and hyperpolarized the resting membrane potential of fast and slow motoneurons, albeit to a much smaller extent in slow motoneurons. These data suggest that a significant resting h-current delays recruitment of fast motoneurons by acting as a shunting conductance. Recruitment may be further delayed due to the progressive loss of inward h-current during depolarization of the membrane potential. Overall, this further refinement of motoneuron subtype recruitment due to changes in Ih during the third postnatal week may not only support orderly recruitment but may also be important for decreasing the recruitment

gain of the motoneuron pool to support complex motor behaviours that require a higher degree of precision compared to earlier developmental stages (Figure 7).

Our analysis provides novel insight into mechanisms that underlie the orderly recruitment of motoneuron subtypes and extend our understanding of the mechanisms controlling the gradation of muscle force beyond the size principle. Motoneuron subtypes also differ in synaptic properties including the circuit of origin, synaptic weight, and neurotransmitter release dynamics [65,67,99,100]. It is likely that functionally specified motor pools may rely on varying degrees of synaptic and intrinsic properties to tune recruitment gain. Furthermore, differential control of intrinsic and synaptic properties of motoneuron subtypes by neuromodulators likely also adjust recruitment gain within motor pools [101,102]. Given the new roles that we show here for PICs and Ih in the differential control of motoneuron subtypes, it is possible that neuromodulation of these currents [16,55,103–106], as descending sources of neuromodulators reach the lumbar spinal cord during development [107,108], may not only shape the emergence of orderly recruitment [109–113], but also provide a means to dynamically modulate recruitment gain.

We set out to identify key intrinsic properties, and the underlying currents, that shape motoneuron recruitment and aimed to determine when these currents are integrated during postnatal development to establish recruitment order amongst motoneuron subtypes. Our results support the notion that fast motoneurons are not simply scaled up slow motoneurons [33]. While passive properties linked to motoneuron size do help to stagger the recruitment of fast and slow motoneurons, we also reveal a key role for active properties, produced by PICs and Ih, which are sequentially integrated during the first three weeks of postnatal development in parallel with the emergence of increasingly complex motor behaviours. Our work will inform future studies aimed toward understanding mechanisms that enable the balance of motor control to shift between the generation of vigorous movements versus precision movements, as is needed during development and when adapting to different motor tasks.

**Acknowledgements**: We are grateful for guidance from Dr. Marco Beato and Dr. Filipe Nascimento on approaches to prepare lumbar slices from functionally mature mice and Frankie Sorrell for comments on an earlier version of the manuscript.

**Funding:** We acknowledge fellowship support to SAS from the Natural Sciences and Engineering Research Council of Canada (NSERC-PDF-517295-2018) and the Royal Society (Newton International Fellowship: NIF/R1/180091).

**Contributions:** S.A.S, performed experiments, analyzed the data, prepared figures, and wrote the first draft of the manuscript. S.A.S. and G.B.M conceived and designed the research, interpreted results, and revised and approved the final version of the manuscript.

## Methods

*Animals*

Experiments were performed on tissue obtained from 113 (male: n = 58; and female: n = 55) wild type C57 Black J/6 mice at postnatal days (P) 1-20. All procedures performed were conducted in accordance with the UK Animals (Scientific Procedures) Act 1986 and were approved by the University of St Andrews Animal Welfare Ethics Committee.

*Tissue preparation*

All animals were sacrificed by performing a cervical dislocation followed by rapid decapitation. Animals were eviscerated and pinned ventral side up in a dissecting chamber lined with silicone elastomer (Sylguard) filled with carbogenated (95% oxygen, 5% carbon dioxide), ice-cold (1-2 degrees Celsius) potassium gluconate based dissecting/slicing aCSF (containing in mM: 130 K-gluconate, 15 KCl, 0.05 EGTA, 20 HEPES, 25 D-glucose, 3 kynurenic acid, 2 Na-pyruvate, 3 myo-inositol, 1 Na-L-ascorbate; pH 7.4, adjusted with NaOH; osmolarity approximately 345 mOsm). Spinal cords were exposed by performing a ventral laminectomy, cutting the ventral roots and gently lifting the spinal cord from the spinal column. Spinal cords were removed within 3 - 5 minutes following cervical dislocation. Spinal cords were secured directly to an agar block (3 % agar) with VetBond surgical glue (3M) and glued to the base of the slicing chamber with cyanoacrylate adhesive. The tissue was immersed in pre-carbogenated ice-cold dissecting/slicing aCSF. Blocks of frozen slicing solution were also placed in the slicing chamber to keep the solution around 1-2 degrees Celsius. On average, the first slice was obtained within 10 minutes of decapitation which increased the likelihood of obtaining viable motoneurons in slices. 300 µm transverse slices were cut at a speed of 10 um/s on the vibratome (Leica VT1200) to minimize tissue compression during slicing. Slices were transferred to a recovery chamber filled with carbogenated pre-warmed (35 degrees Celsius) recovery aCSF (containing in mM: 119 NaCl, 1.9 KCl, 1.2 NaH2PO4, 10 MgSO4, 1 CaCl, 26 NaHCO3, 20 glucose, 1.5 kynurenic acid, 3% dextran) for thirty minutes after completion of the last slice which took 10 -15 minutes on average. Following recovery, slices were transferred to a chamber filled with carbogenated warm (35 degrees Celsius) recording aCSF (containing in mM: 127 NaCl, 3 KCl, 1.25 NaH2PO4, 1 MgCl, 2 CaCl2, 26 NaHCO3, 10 glucose) and allowed to equilibrate at room temperature (maintained at 23-25 degrees Celsius) for at least one hour before experiments were initiated.

*Whole cell patch clamp electrophysiology*

Whole cell patch clamp recordings were obtained from 308 lumbar motoneurons. Slices were stabilized in a recording chamber with fine fibres secured to a platinum harp and visualized with a 40x objective with infrared illumination and differential interference contrast. A large proportion of the motoneurons studied were identified based on location in the ventrolateral region with somata greater than 20 µm. Recordings were obtained from a subset of motoneurons that had been retrogradely labelled with Fluorogold (Fluorochrome, Denver, CO). Fluorogold was dissolved in sterile saline solution and 0.04 mg/g injected intraperitoneally 24-48 hours prior to experiments [93]. In addition to recording from larger FG-positive cells, this approach allowed us to more confidently target smaller motoneurons. Motoneurons were visualized and whole cell recordings obtained under DIC illumination with pipettes (L: 100 mm, OD: 1.5 mm, ID: 0.84 mm; World Precision Instruments) pulled on a Flaming Brown micropipette puller (Sutter instruments P97) to a resistance of 2.5-3.5 MΩ. Pipettes were back-filled with intracellular solution (containing in mM: 140 KMeSO4, 10 NaCl, 1 CaCl2, 10 HEPES, 1 EGTA, 3 Mg-ATP and 0.4 GTP-Na2; pH 7.2-7.3, adjusted with KOH).

Signals were amplified and filtered (6 kHz low pass Bessel filter) with a Multiclamp 700 B amplifier, acquired at 20 kHz using a Digidata 1440A digitizer with pClamp Version 10.7 software (Molecular Devices) and stored on a computer for offline analysis.

*Identification of fast and slow motoneuron types*

Fast and slow motoneurons were identified using a protocol established by Leroy et al., [27,28], which differentiates motoneuron type based on the latency to the first spike when injecting a 5 second square depolarizing current near the threshold for repetitive firing. Using this approach we were able to identify 2 main firing profiles - a delayed repetitive firing profile with accelerating spike frequency, characteristic of fast-type motoneurons, and an immediate firing profile with little change in spike frequency, characteristic of slow-type motoneurons (Figure 1; [27,28]). Delayed and immediate firing motoneurons were identified in equal proportions at each developmental time point studied (Week 1: Delayed: 58% Immediate: 42%; Week 2: Delayed: 67% Immediate: 33%; Week 3: Delayed: 65% Immediate: 35%) and were found in rostral and caudal segments of male and female mice. There were no apparent differences in the relative proportions of the two motoneuron types when comparing spinal segment or sex. Data analysis was performed whilst blinded to motoneuron subtype.

All motoneuron intrinsic properties were studied by applying a bias current to maintain the membrane potential at -60 mV, or at -70 mV for the subset of experiments with ZD-7288. Values reported are not liquid junction potential corrected to facilitate comparisons with previously published data [20,29,109,114–116]. Cells were excluded from analysis if access resistance was greater than 20 MΩ or changed by more than 5 MΩ over the duration of the recording, if resting membrane potential deviated by more than 5 mV over the duration of the recording period, or if spike amplitude measured from threshold (described below) was less than 60 mV.

*Pharmacology*

We deploy pharmacological tools to probe the contribution of ion channels contributing to persistent inward currents (PICs) and hyperpolarization activated inward currents (Ih). Nifedipine (20 µM; Tocris) was used to assess the contribution of L-type calcium channels, and 4,9 - Anhydro Tetrodotoxin (200 nM; Tocris) to assess the contribution of NaV1.6 channels to PIC and recruitment. Ih was blocked with the selective HCN channel blocker, ZD-7288 (10 µM; Tocris).

*Data acquisition and analysis*

Passive properties including capacitance, membrane time constant (tau), and passive input resistance (Ri) were measured during a hyperpolarizing current pulse that brought the membrane potential from -60 to -70mV. Input resistance was measured from the initial voltage trough to minimize the impact of slower acting active conductances (eg. Ih, sag). The time constant was measured as the time it took to reach 2/3 of the peak voltage change. Capacitance was calculated by dividing the time constant by the input resistance (C=T/R). Resting membrane potential was measured 10 minutes after obtaining a whole cell configuration and at the end of recordings from the MultiClamp Commander.

Recruitment and repetitive firing properties were assessed during slow (100 pA/s) depolarizing current ramps which allowed us to measure the recruitment current and voltage threshold of the first action potential. Recruitment gain was qualitatively illustrated by generating cumulative proportion histograms of recruitment current values across respective motoneuron samples at developmental time points or before and after drug application. The voltage threshold of the first action potential was defined when the change in voltage reached 10 mV/ms. Firing rates were measured at recruitment, 2 times recruitment current, and derecruitment (maximum firing rate). As previously reported, motoneurons

displayed sub primary and primary regions of the FI relationship. Sub primary range gain was measured from the slope of a linear function fitted to the initial section of the FI relationship [61,62,117]. We did not find evidence for a secondary firing range in the motoneurons studied.

The subthreshold trajectory of the membrane potential measured in response to a slow depolarizing current ramp is composed of passive and active elements defined by linear and exponential changes in membrane potential respectively [36,38,39]. The slope of this linear phase was calculated as a proxy for passive excitability. The onset of the active, exponential component of the membrane depolarisation was defined as the point at which the membrane potential deviated by more than 1mV from the linear function of the passive phase. The current and voltage values at the onset of the voltage acceleration were compared to the rheobase current and voltage threshold measured from the first action potential elicited on the depolarising current ramp. A hypothetical 'passive recruitment' current was then estimated by extrapolating the line applied to the passive depolarising phase and measuring its intersection with the voltage threshold of the first spike. The difference between this hypothetical passive recruitment current and the measured recruitment current was calculated to quantify the influence that active conductances (presumably persistent inward current) have on recruitment.

The influence that persistent inward currents (PICs) exert on motoneuron excitability was also estimated in current clamp mode using the injection of a triangular, depolarizing current ramp with 5 second rise and fall times [18,28,29,118]. Depolarizing current ramps were set to a peak current of 2 times repetitive firing threshold current (determined with a 100pA/s depolarizing current ramp initiated from -60 mV). The influence of persistent inward currents on motoneuron excitability was estimated by calculating the difference (delta I) between the current at firing onset on the ascending component of the ramp and the current at derecruitment on the descending component of the ramp. A negative delta I is suggestive of a PIC. Firing hysteresis was also assessed on the ascending and descending components of the ramp. We subdivided cells into 1 of 4 types based on the firing hysteresis on ascending and descending portions of the ramp [18,29,119,120] (Type 1: Linear, Type 2: Adapting, Type 3: Sustained, Type 4: Counter clockwise).

PICs were measured in voltage clamp by injecting a slow depolarizing voltage ramp (10 mV/s from -90 to -10 mV) over 8 seconds [20,118,121]. PIC onset voltage, voltage at which the peak current occurs (voltage peak), peak current amplitude, and peak current density were measured from post-hoc leak-subtracted traces as in [20,118,122].

Input resistance was calculated by taking the slope of the current-voltage relationship at initial (peak voltage trough at the start) and steady state (plateau at end) voltage deflection during a series of 1 second hyperpolarizing current steps. Sag conductances were estimated as the difference in conductance (1/R) measured during initial and steady state voltage plateau at the end of hyperpolarizing current steps ($(1/Rin_{ss}) - (1/Rin_{initial})$). Ih was measured in voltage clamp during 1 second hyperpolarizing voltage steps from - 60 mV to - 110 mV, in 10 mV increments. Ih was measured as the difference between the initial and steady state current within similar windows analyzed for depolarizing sag in current clamp. Ih time constant (tau) was measured as the time (in ms) to reach 2/3 peak Ih at each respective voltage step.

Single spike (spike threshold, amplitude, rise time, half width) and afterhyperpolarization (AHP) (amplitude and half width) were elicited using a 10 ms square, depolarising current pulse applied at an intensity 25% above rheobase current. Spike threshold was determined as the potential at which the derivative (dV/dt) increased above 10 mV/ms. Spike amplitude, rise time and half width were measured

from this point. Medium afterhyperpolarization (mAHP) properties (amplitude and half width) were measured from baseline (-60 mV). Single spike and mAHP properties were measured using event detection features in Clampfit Version 11 (Molecular Devices).

*Research design and statistical analysis*

Two factor analysis of variance (ANOVA) was performed with motoneuron type (Fast and Slow) and postnatal week (Week 1, 2, 3) as factors to address 3 core questions for each parameter studied: 1.) Was there a difference between subtypes? 2.) Did it change during development? 3.) Do the subtypes mature differently during development? Statistical results addressing these questions are listed sequentially in Supplementary Table 1: 1: Main effect of subtype; 2: main effect of development; 3: Subtype x development interaction. Holm Sidak post hoc analysis was performed when significant main effects or interactions were detected with a significance level of $p < 0.05$ and are all summarized in Supplementary Table 1. Pearson correlations were performed between recruitment current and passive properties (Gustafson and Pinter, 1984), within each motoneuron subtype at each week. A simple linear regression, comparing the slopes of fast and slow motoneurons, was used to determine the degree of similarities, or differences for each of the analyses performed (Figure 3). Two factor repeated measures ANOVA were conducted to test the effect of pharmacological agents on intrinsic properties and currents with MN type and drug as factors. Appropriate and equivalent nonparametric tests (Mann-Whitney or Kruskal-Wallis) were conducted when data failed tests of normality or equal variance with Shapiro Wilk and Brown-Forsythe tests, respectively. Individual data points for all cells are presented in figures with mean ± SD. Statistical analyses were performed using Graph Pad Version 9.0 (Prism, San Diego, CA, USA).

Principle component analysis was performed using GraphPad Version 9.0 to determine global changes in motoneuron intrinsic properties during the first three weeks of postnatal development. 25 intrinsic properties from 261 motoneurons across weeks 1, 2, and 3 were included in the analysis. Principle component scores (PC Scores) for each cell were extracted for each Principle Component and changes between subtypes during development were analyzed using a 2 factor ANOVA. 3D scatterplots between PC scores (PCs 1-3) were generated in Sigmaplot 14.0 (Sigmastat, San Jose, CA, USA).

**References**


1. Liddell, E.G.T., and Sherrington, S.C.S. (1924*). Further Observations on Myotatic Reflexes.

2. Burke, R.E., Levine, D.N., Tsairis, P., and Zajac, F.E., 3rd (1973). Physiological types and histochemical profiles in motor units of the cat gastrocnemius. J. Physiol. *234*, 723–748.

3. Henneman, E. (1957). Relation between size of neurons and their susceptibility to discharge. Science *126*, 1345–1347.

4. Somjen, G., Carpenter, D.O., and Henneman, E. (1965). Responses of motoneurons of different sizes to graded stimulation of supraspinal centers of the brain. J. Neurophysiol. *28*, 958–965.

5. Burke, R.E., Dum, R.P., Fleshman, J.W., Glenn, L.L., Lev-Tov, A., O'Donovan, M.J., and Pinter, M.J. (1982). A HRP study of the relation between cell size and motor unit type in cat ankle extensor motoneurons. J. Comp. Neurol. *209*, 17–28.

6. Gustafsson, B., and Pinter, M.J. (1984). Relations among passive electrical properties of lumbar alpha-motoneurones of the cat. J. Physiol. *356*, 401–431.

7. Zengel, J.E., Reid, S.A., Sypert, G.W., and Munson, J.B. (1985). Membrane electrical properties and prediction of motor-unit type of medial gastrocnemius motoneurons in the cat. J. Neurophysiol. *53*, 1323–1344.

8. Zajac, F.E., and Faden, J.S. (1985). Relationship among recruitment order, axonal conduction velocity, and muscle-unit properties of type-identified motor units in cat plantaris muscle. J. Neurophysiol. *53*, 1303–1322.

9. Cope, T.C., and Clark, B.D. (1991). Motor-unit recruitment in the decerebrate cat: several unit properties are equally good predictors of order. J. Neurophysiol. *66*, 1127–1138.

10. Cope, T.C., and Pinter, M.J. (1995). The Size Principle: Still Working After All These Years. Physiology *10*, 280–286.

11. Brocard, F. (2019). New channel lineup in spinal circuits governing locomotion. Current Opinion in Physiology *8*, 14–22.

12. Deardorff, A.S., Romer, S.H., and Fyffe, R.E.W. (2021). Location, location, location: the organization and roles of potassium channels in mammalian motoneurons. J. Physiol. *599*, 1391–1420.

13. Heckman, C.J., Hyngstrom, A.S., and Johnson, M.D. (2008). Active properties of motoneurone dendrites: diffuse descending neuromodulation, focused local inhibition. J. Physiol. *586*, 1225–1231.

14. Schwindt, P.C., and Crill, W.E. (1980). Properties of a persistent inward current in normal and TEA-injected motoneurons. J. Neurophysiol. *43*, 1700–1724.

15. Hounsgaard, J., and Kiehn, O. (1993). Calcium spikes and calcium plateaux evoked by differential polarization in dendrites of turtle motoneurones in vitro. J. Physiol. *468*, 245–259.

16. Hounsgaard, J., Hultborn, H., Jespersen, B., and Kiehn, O. (1988). Bistability of alpha-motoneurones in the decerebrate cat and in the acute spinal cat after intravenous 5-hydroxytryptophan. The Journal of Physiology *405*, 345–367.

17. Lee, R.H., and Heckman, C.J. (1998). Bistability in Spinal Motoneurons In Vivo: Systematic Variations in Persistent Inward Currents. Journal of Neurophysiology *80*, 583–593.

18. Li, Y., and Bennett, D.J. (2003). Persistent Sodium and Calcium Currents Cause Plateau Potentials in Motoneurons of Chronic Spinal Rats. Journal of Neurophysiology *90*, 857–869.

19. Chatelier, A., Zhao, J., Bois, P., and Chahine, M. (2010). Biophysical characterisation of the persistent sodium current of the Nav1.6 neuronal sodium channel: a single-channel analysis. Pflugers Arch. *460*, 77–86.

20. Quinlan, K.A., Schuster, J.E., Fu, R., Siddique, T., and Heckman, C.J. (2011). Altered postnatal maturation of electrical properties in spinal motoneurons in a mouse model of amyotrophic lateral sclerosis. J. Physiol. *589*, 2245–2260.

21. Brocard, C., Plantier, V., Boulenguez, P., Liabeuf, S., Bouhadfane, M., Viallat-Lieutaud, A., Vinay, L., and Brocard, F. (2016). Cleavage of Na(+) channels by calpain increases persistent Na(+) current and promotes spasticity after spinal cord injury. Nat. Med. *22*, 404–411.

22. Schwindt, P., and Crill, W.E. (1977). A persistent negative resistance in cat lumbar motoneurons. Brain Res. *120*, 173–178.

23. Heckman, C.J., Johnson, M., Mottram, C., and Schuster, J. (2008). Persistent inward currents in spinal motoneurons and their influence on human motoneuron firing patterns. Neuroscientist *14*, 264–275.

24. Bos, R., Harris-Warrick, R.M., Brocard, C., Demianenko, L.E., Manuel, M., Zytnicki, D., Korogod, S.M., and Brocard, F. (2018). Kv1.2 Channels Promote Nonlinear Spiking Motoneurons for Powering Up Locomotion. Cell Rep. *22*, 3315–3327.

25. Soulard, C., Salsac, C., Mouzat, K., Hilaire, C., Roussel, J., Mezghrani, A., Lumbroso, S., Raoul, C., and Scamps, F. (2020). Spinal Motoneuron TMEM16F Acts at C-boutons to Modulate Motor Resistance and Contributes to ALS Pathogenesis. Cell Rep. *30*, 2581–2593.e7.

26. Zhang, Q., and Dai, Y. (2020). A modeling study of spinal motoneuron recruitment regulated by ionic channels during fictive locomotion. Journal of Computational Neuroscience *48*, 409–428.

27. Leroy, F., Lamotte d'Incamps, B., Imhoff-Manuel, R.D., and Zytnicki, D. (2014). Early intrinsic hyperexcitability does not contribute to motoneuron degeneration in amyotrophic lateral sclerosis. Elife *3*.

28. Leroy, F., Lamotte d'Incamps, B., and Zytnicki, D. (2015). Potassium currents dynamically set the recruitment and firing properties of F-type motoneurons in neonatal mice. J. Neurophysiol. *114*, 1963–1973.

29. Durand, J., Filipchuk, A., Pambo-Pambo, A., Amendola, J., Borisovna Kulagina, I., and Guéritaud, J.-P. (2015). Developing electrical properties of postnatal mouse lumbar motoneurons. Front. Cell. Neurosci. *9*, 349.

30. Bhumbra, G.S., and Beato, M. (2018). Recurrent excitation between motoneurones propagates across segments and is purely glutamatergic. PLoS Biol. *16*, e2003586.

31. Brocard, F., Vinay, L., and Clarac, F. (1999). Development of hindlimb postural control during the first postnatal week in the rat. Brain Res. Dev. Brain Res. *117*, 81–89.

32. Altman, J., and Sudarshan, K. (1975). Postnatal development of locomotion in the laboratory rat. Anim. Behav. *23*, 896–920.

33. Kernell, D., and Zwaagstra, B. (1981). Input conductance axonal conduction velocity and cell size among hindlimb motoneurones of the cat. Brain Res. *204*, 311–326.

34. Gardiner, P.F. (1993). Physiological properties of motoneurons innervating different muscle unit types in rat gastrocnemius. J. Neurophysiol. *69*, 1160–1170.

35. Martínez-Silva, M. de L., Imhoff-Manuel, R.D., Sharma, A., Heckman, C.J., Shneider, N.A., Roselli, F., Zytnicki, D., and Manuel, M. (2018). Hypoexcitability precedes denervation in the large fast-contracting motor units in two unrelated mouse models of ALS. Elife *7*.

36. Kuo, J.J., Lee, R.H., Zhang, L., and Heckman, C.J. (2006). Essential role of the persistent sodium current in spike initiation during slowly rising inputs in mouse spinal neurones. J. Physiol. *574*, 819–834.

37. Iglesias, C., Meunier, C., Manuel, M., Timofeeva, Y., Delestree, N., and Zytnicki, D. (2011). Mixed Mode Oscillations in Mouse Spinal Motoneurons Arise from a Low Excitability State. Journal of Neuroscience *31*, 5829–5840.

38. Delestrée, N., Manuel, M., Iglesias, C., Elbasiouny, S.M., Heckman, C.J., and Zytnicki, D. (2014). Adult spinal motoneurones are not hyperexcitable in a mouse model of inherited amyotrophic lateral sclerosis. J. Physiol. *592*, 1687–1703.

39. Jørgensen, H.S., Jensen, D.B., Dimintiyanova, K.P., Bonnevie, V.S., Hedegaard, A., Lehnhoff, J., Moldovan, M., Grondahl, L., and Meehan, C.F. (2020). Increased Axon Initial Segment Length Results in Increased Na Currents in Spinal Motoneurones at Symptom Onset in the G127X SOD1 Mouse Model of Amyotrophic Lateral Sclerosis. Neuroscience.

40. Harvey, P.J., Li, X., Li, Y., and Bennett, D.J. (2006). 5-HT2 receptor activation facilitates a persistent sodium current and repetitive firing in spinal motoneurons of rats with and without chronic spinal cord injury. J. Neurophysiol. *96*, 1158–1170.

41. Krzemien, D.M., Schaller, K.L., Levinson, S.R., and Caldwell, J.H. (2000). Immunolocalization of sodium channel isoform NaCh6 in the nervous system. J. Comp. Neurol. *420*, 70–83.

42. Schaller, K.L., and Caldwell, J.H. (2000). Developmental and regional expression of sodium channel isoform NaCh6 in the rat central nervous system. J. Comp. Neurol. *420*, 84–97.

43. Zhang, M., Sukiasyan, N., Møller, M., Bezprozvanny, I., Zhang, H., Wienecke, J., and Hultborn, H. (2006). Localization of L-type calcium channel Ca(V)1.3 in cat lumbar spinal cord--with emphasis on motoneurons. Neurosci. Lett. *407*, 42–47.

44. Anelli, R., Sanelli, L., Bennett, D.J., and Heckman, C.J. (2007). Expression of L-type calcium channel alpha(1)-1.2 and alpha(1)-1.3 subunits on rat sacral motoneurons following chronic spinal cord injury. Neuroscience *145*, 751–763.

45. Li, Y., Gorassini, M.A., and Bennett, D.J. (2004). Role of persistent sodium and calcium currents in motoneuron firing and spasticity in chronic spinal rats. J. Neurophysiol. *91*, 767–783.

46. Perrier, J.F., and Hounsgaard, J. (1999). Ca(2+)-activated nonselective cationic current (I(CAN)) in turtle motoneurons. J. Neurophysiol. *82*, 730–735.

47. Bouhadfane, M., Tazerart, S., Moqrich, A., Vinay, L., and Brocard, F. (2013). Sodium-mediated plateau potentials in lumbar motoneurons of neonatal rats. J. Neurosci. *33*, 15626–15641.

48. Wilson, J.M., Hartley, R., Maxwell, D.J., Todd, A.J., Lieberam, I., Kaltschmidt, J.A., Yoshida, Y., Jessell, T.M., and Brownstone, R.M. (2005). Conditional rhythmicity of ventral spinal interneurons defined by expression of the Hb9 homeodomain protein. J. Neurosci. *25*, 5710–5719.

49. Dougherty, K.J., and Kiehn, O. (2010). Firing and cellular properties of V2a interneurons in the

rodent spinal cord. J. Neurosci. *30*, 24–37.

50. Zhong, G., Droho, S., Crone, S.A., Dietz, S., Kwan, A.C., Webb, W.W., Sharma, K., and Harris-Warrick, R.M. (2010). Electrophysiological characterization of V2a interneurons and their locomotor-related activity in the neonatal mouse spinal cord. J. Neurosci. *30*, 170–182.

51. Engbers, J.D.T., Anderson, D., Tadayonnejad, R., Mehaffey, W.H., Molineux, M.L., and Turner, R.W. (2011). Distinct roles for I(T) and I(H) in controlling the frequency and timing of rebound spike responses. J. Physiol. *589*, 5391–5413.

52. McLarnon, J.G. (1995). Potassium currents in motoneurones. Prog. Neurobiol. *47*, 513–531.

53. Bayliss, D.A., Viana, F., Bellingham, M.C., and Berger, A.J. (1994). Characteristics and postnatal development of a hyperpolarization-activated inward current in rat hypoglossal motoneurons in vitro. J. Neurophysiol. *71*, 119–128.

54. Kiehn, O., Kjaerulff, O., Tresch, M.C., and Harris-Warrick, R.M. (2000). Contributions of intrinsic motor neuron properties to the production of rhythmic motor output in the mammalian spinal cord. Brain Res. Bull. *53*, 649–659.

55. Kjaerulff, O., and Kiehn, O. (2001). 5-HT modulation of multiple inward rectifiers in motoneurons in intact preparations of the neonatal rat spinal cord. J. Neurophysiol. *85*, 580–593.

56. Perrier, J.-F., Alaburda, A., and Hounsgaard, J. (2003). 5-HT1A receptors increase excitability of spinal motoneurons by inhibiting a TASK-1-like K+ current in the adult turtle. J. Physiol. *548*, 485–492.

57. Araki, T., Ito, M., and Oshima, T. (1961). Potential changes produced by application of current steps in motoneurones. Nature *191*, 1104–1105.

58. Ito, M., and Oshima, T. (1965). Electrical behaviour of the motoneurone membrane during intracellularly applied current steps. J. Physiol. *180*, 607–635.

59. Burke, R.E., and ten Bruggencate, G. (1971). Electrotonic characteristics of alpha motoneurones of varying size. The Journal of Physiology *212*, 1–20.

60. Takahashi, T. (1990). Inward rectification in neonatal rat spinal motoneurones. J. Physiol. *423*, 47–62.

61. Manuel, M., Iglesias, C., Donnet, M., Leroy, F., Heckman, C.J., and Zytnicki, D. (2009). Fast kinetics, high-frequency oscillations, and subprimary firing range in adult mouse spinal motoneurons. J. Neurosci. *29*, 11246–11256.

62. Meehan, C.F., Sukiasyan, N., Zhang, M., Nielsen, J.B., and Hultborn, H. (2010). Intrinsic properties of mouse lumbar motoneurons revealed by intracellular recording in vivo. J. Neurophysiol. *103*, 2599–2610.

63. Kernell, D., and Hultborn, H. (1990). Synaptic effects on recruitment gain: a mechanism of importance for the input-output relations of motoneurone pools? Brain Res. *507*, 176–179.

64. Nielsen, J.B., Morita, H., Wenzelburger, R., Deuschl, G., Gossard, J.-P., and Hultborn, H. (2019). Recruitment gain of spinal motor neuron pools in cat and human. Exp. Brain Res. *237*, 2897–2909.

65. McLean, D.L., Fan, J., Higashijima, S.-I., Hale, M.E., and Fetcho, J.R. (2007). A topographic map of recruitment in spinal cord. Nature *446*, 71–75.

66. Ampatzis, K., Song, J., Ausborn, J., and El Manira, A. (2013). Pattern of innervation and recruitment of different classes of motoneurons in adult zebrafish. J. Neurosci. *33*, 10875–10886.

67. Gabriel, J.P., Ausborn, J., Ampatzis, K., Mahmood, R., Eklöf-Ljunggren, E., and El Manira, A. (2011). Principles governing recruitment of motoneurons during swimming in zebrafish. Nature Neuroscience *14*, 93–99.

68. Zwart, M.F., Pulver, S.R., Truman, J.W., Fushiki, A., Fetter, R.D., Cardona, A., and Landgraf, M. (2016). Selective Inhibition Mediates the Sequential Recruitment of Motor Pools. Neuron *91*, 944.

69. Azevedo, A.W., Dickinson, E.S., Gurung, P., Venkatasubramanian, L., Mann, R.S., and Tuthill, J.C. (2020). A size principle for recruitment of leg motor neurons. Elife *9*.

70. Bawa, P., Binder, M.D., Ruenzel, P., and Henneman, E. (1984). Recruitment order of motoneurons in stretch reflexes is highly correlated with their axonal conduction velocity. J. Neurophysiol. *52*, 410–420.

71. Kaplan, A., Spiller, K.J., Towne, C., Kanning, K.C., Choe, G.T., Geber, A., Akay, T., Aebischer, P., and Henderson, C.E. (2014). Neuronal matrix metalloproteinase-9 is a determinant of selective neurodegeneration. Neuron *81*, 333–348.

72. Nijssen, J., Comley, L.H., and Hedlund, E. (2017). Motor neuron vulnerability and resistance in amyotrophic lateral sclerosis. Acta Neuropathol. *133*, 863–885.

73. Fuchs, A., Kutterer, S., Mühling, T., Duda, J., Schütz, B., Liss, B., Keller, B.U., and Roeper, J. (2013). Selective mitochondrial Ca2 uptake deficit in disease endstage vulnerable motoneurons of the SOD1G93Amouse model of amyotrophic lateral sclerosis. The Journal of Physiology *591*, 2723–2745.

74. Dengler, R., Konstanzer, A., Küther, G., Hesse, S., Wolf, W., and Struppler, A. (1990). Amyotrophic lateral sclerosis: macro-EMG and twitch forces of single motor units. Muscle Nerve *13*, 545–550.

75. Thomas, C.K., Bakels, R., Klein, C.S., and Zijdewind, I. (2014). Human spinal cord injury: motor unit properties and behaviour. Acta Physiol. *210*, 5–19.

76. Hu, X., Suresh, A.K., Rymer, W.Z., and Suresh, N.L. (2015). Assessing altered motor unit recruitment patterns in paretic muscles of stroke survivors using surface electromyography. J. Neural Eng. *12*, 066001.

77. Vecchio, A.D., Del Vecchio, A., Sylos-Labini, F., Mondì, V., Paolillo, P., Ivanenko, Y., Lacquaniti, F., and Farina, D. (2020). Spinal motoneurons of the human newborn are highly synchronized during leg movements. Science Advances *6*, eabc3916.

78. Close, R. (1964). DYNAMIC PROPERTIES OF FAST AND SLOW SKELETAL MUSCLES OF THE RAT DURING DEVELOPMENT. J. Physiol. *173*, 74–95.

79. Hanson, M.G., Gartz Hanson, M., and Landmesser, L.T. (2004). Normal Patterns of Spontaneous Activity Are Required for Correct Motor Axon Guidance and the Expression of Specific Guidance Molecules. Neuron *43*, 687–701.

80. Bennett, M.R., McGrath, P.A., Davey, D.F., and Hutchinson, I. (1983). Death of motorneurons during the postnatal loss of polyneuronal innervation of rat muscles. J. Comp. Neurol. *218*, 351–363.

81. Brown, M.C., Jansen, J.K., and Van Essen, D. (1976). Polyneuronal innervation of skeletal

muscle in new-born rats and its elimination during maturation. J. Physiol. *261*, 387–422.

82. Walton, K.D., and Navarrete, R. (1991). Postnatal changes in motoneurone electrotonic coupling studied in the in vitro rat lumbar spinal cord. J. Physiol. *433*, 283–305.

83. Chang, Q., Gonzalez, M., Pinter, M.J., and Balice-Gordon, R.J. (1999). Gap junctional coupling and patterns of connexin expression among neonatal rat lumbar spinal motor neurons. J. Neurosci. *19*, 10813–10828.

84. Personius, K.E., Chang, Q., Mentis, G.Z., O'Donovan, M.J., and Balice-Gordon, R.J. (2007). Reduced gap junctional coupling leads to uncorrelated motor neuron firing and precocious neuromuscular synapse elimination. Proc. Natl. Acad. Sci. U. S. A. *104*, 11808–11813.

85. Nakanishi, S.T., and Whelan, P.J. (2010). Diversification of intrinsic motoneuron electrical properties during normal development and botulinum toxin-induced muscle paralysis in early postnatal mice. J. Neurophysiol. *103*, 2833–2845.

86. Vinay, L., Brocard, F., Pflieger, J.F., Simeoni-Alias, J., and Clarac, F. (2000). Perinatal development of lumbar motoneurons and their inputs in the rat. Brain Res. Bull. *53*, 635–647.

87. Carrascal, L., Nieto-Gonzalez, J.L., Cameron, W.E., Torres, B., and Nunez-Abades, P.A. (2005). Changes during the postnatal development in physiological and anatomical characteristics of rat motoneurons studied in vitro. Brain Res. Brain Res. Rev. *49*, 377–387.

88. Li, Y., Brewer, D., Burke, R.E., and Ascoli, G.A. (2005). Developmental changes in spinal motoneuron dendrites in neonatal mice. The Journal of Comparative Neurology *483*, 304–317.

89. Fleshman, J.W., Munson, J.B., Sypert, G.W., and Friedman, W.A. (1981). Rheobase, input resistance, and motor-unit type in medial gastrocnemius motoneurons in the cat. J. Neurophysiol. *46*, 1326–1338.

90. Hounsgaard, J., and Kiehn, O. (1989). Serotonin-induced bistability of turtle motoneurones caused by a nifedipine-sensitive calcium plateau potential. J. Physiol. *414*, 265–282.

91. Carlin, K.P., Bui, T.V., Dai, Y., and Brownstone, R.M. (2009). Staircase currents in motoneurons: insight into the spatial arrangement of calcium channels in the dendritic tree. J. Neurosci. *29*, 5343–5353.

92. Carlin, K.P., Jones, K.E., Jiang, Z., Jordan, L.M., and Brownstone, R.M. (2000). Dendritic L-type calcium currents in mouse spinal motoneurons: implications for bistability. Eur. J. Neurosci. *12*, 1635–1646.

93. Miles, G.B., Dai, Y., and Brownstone, R.M. (2005). Mechanisms underlying the early phase of spike frequency adaptation in mouse spinal motoneurones. J. Physiol. *566*, 519–532.

94. Lee, R.H., and Heckman, C.J. (1998). Bistability in Spinal Motoneurons In Vivo: Systematic Variations in Rhythmic Firing Patterns. Journal of Neurophysiology *80*, 572–582.

95. Rotterman, T.M., Carrasco, D., Housley, N., Nardelli, P., Powers, R.K., and Cope, T.C. (2021). Somatic Proximity of the Axon Initial Segment Predicts Motoneuron Excitability.

96. Milligan, C.J., Edwards, I.J., and Deuchars, J. (2006). HCN1 ion channel immunoreactivity in spinal cord and medulla oblongata. Brain Res. *1081*, 79–91.

97. Tsuzuki, S., Yoshida, S., Yamamoto, T., and Oka, H. (1995). Developmental changes in the electrophysiological properties of neonatal rat oculomotor neurons studied in vitro. Neurosci. Res. *23*, 389–397.

98. Russier, M., Carlier, E., Ankri, N., Fronzaroli, L., and Debanne, D. (2003). A-, T-, and H-type currents shape intrinsic firing of developing rat abducens motoneurons. J. Physiol. *549*, 21–36.

99. Song, J., Pallucchi, I., Ausborn, J., Ampatzis, K., Bertuzzi, M., Fontanel, P., Picton, L.D., and El Manira, A. (2020). Multiple Rhythm-Generating Circuits Act in Tandem with Pacemaker Properties to Control the Start and Speed of Locomotion. Neuron *105*, 1048–1061.e4.

100. Binder, M.D., Heckman, C.J., and Powers, R.K. (2002). Relative strengths and distributions of different sources of synaptic input to the motoneurone pool: implications for motor unit recruitment. Adv. Exp. Med. Biol. *508*, 207–212.

101. Bertuzzi, M., and Ampatzis, K. (2018). Spinal cholinergic interneurons differentially control motoneuron excitability and alter the locomotor network operational range. Sci. Rep. *8*, 1988.

102. Jha, U., and Thirumalai, V. Neuromodulatory selection of motor neuron recruitment patterns in a visuomotor behavior increases speed.

103. Harvey, P.J., Li, X., Li, Y., and Bennett, D.J. (2006). Endogenous Monoamine Receptor Activation Is Essential for Enabling Persistent Sodium Currents and Repetitive Firing in Rat Spinal Motoneurons. Journal of Neurophysiology *96*, 1171–1186.

104. Revill, A.L., Chu, N.Y., Ma, L., LeBlancq, M.J., Dickson, C.T., and Funk, G.D. (2019). Postnatal development of persistent inward currents in rat XII motoneurons and their modulation by serotonin, muscarine and noradrenaline. J. Physiol. *597*, 3183–3201.

105. Conway, B.A., Hultborn, H., Kiehn, O., and Mintz, I. (1988). Plateau potentials in alpha-motoneurones induced by intravenous injection of L-dopa and clonidine in the spinal cat. J. Physiol. *405*, 369–384.

106. Sirois, J.E., Lynch, C., 3rd, and Bayliss, D.A. (2002). Convergent and reciprocal modulation of a leak K+ current and I(h) by an inhalational anaesthetic and neurotransmitters in rat brainstem motoneurones. J. Physiol. *541*, 717–729.

107. Bregman, B.S. (1987). Development of serotonin immunoreactivity in the rat spinal cord and its plasticity after neonatal spinal cord lesions. Brain Res. *431*, 245–263.

108. Commissiong, J.W. (1983). The development of catecholaminergic nerves in the spinal cord of rat. II. Regional development. Brain Res. *313*, 75–92.

109. Smith, C.C., and Brownstone, R.M. (2020). Spinal motoneuron firing properties mature from rostral to caudal during postnatal development of the mouse. J. Physiol. *598*, 5467–5485.

110. Vinay, L., Ben-Mabrouk, F., Brocard, F., Clarac, F., Jean-Xavier, C., Pearlstein, E., and Pflieger, J.-F. (2005). Perinatal development of the motor systems involved in postural control. Neural Plast. *12*, 131–9; discussion 263–72.

111. Vinay, L., Brocard, F., and Clarac, F. (2000). Differential maturation of motoneurons innervating ankle flexor and extensor muscles in the neonatal rat. European Journal of Neuroscience *12*, 4562–4566.

112. Vinay, L., Brocard, F., Clarac, F., Norreel, J.C., Pearlstein, E., and Pflieger, J.F. (2002). Development of posture and locomotion: an interplay of endogenously generated activities and neurotrophic actions by descending pathways. Brain Res. Brain Res. Rev. *40*, 118–129.

113. Pflieger, J.-F., Clarac, F., and Vinay, L. (2002). Postural modifications and neuronal excitability changes induced by a short-term serotonin depletion during neonatal development in the rat. J. Neurosci. *22*, 5108–5117.

114. Nascimento, F., Spindler, L.R.B., and Miles, G.B. (2019). Balanced cholinergic modulation of spinal locomotor circuits via M2 and M3 muscarinic receptors. Sci. Rep. *9*, 14051.

115. Nascimento, F., Broadhead, M.J., Tetringa, E., Tsape, E., Zagoraiou, L., and Miles, G.B. (2020). Synaptic mechanisms underlying modulation of locomotor-related motoneuron output by premotor cholinergic interneurons. Elife *9*.

116. Miles, G.B., Hartley, R., Todd, A.J., and Brownstone, R.M. (2007). Spinal cholinergic interneurons regulate the excitability of motoneurons during locomotion. Proc. Natl. Acad. Sci. U. S. A. *104*, 2448–2453.

117. Jensen, D.B., Stecina, K., Wienecke, J., Hedegaard, A., Sukiasyan, N., Hultborn, H.R., and Meehan, C.F. (2018). The Subprimary Range of Firing Is Present in Both Cat and Mouse Spinal Motoneurons and Its Relationship to Force Development Is Similar for the Two Species. J. Neurosci. *38*, 9741–9753.

118. Steele, P.R., Cavarsan, C.F., Dowaliby, L., Westefeld, M., Katenka, N., Drobyshevsky, A., Gorassini, M.A., and Quinlan, K.A. (2020). Altered Motoneuron Properties Contribute to Motor Deficits in a Rabbit Hypoxia-Ischemia Model of Cerebral Palsy. Front. Cell. Neurosci. *14*, 69.

119. Cotel, F., Antri, M., Barthe, J.-Y., and Orsal, D. (2009). Identified ankle extensor and flexor motoneurons display different firing profiles in the neonatal rat. J. Neurosci. *29*, 2748–2753.

120. Bennett, D.J., Hultborn, H., Fedirchuk, B., and Gorassini, M. (1998). Short-term plasticity in hindlimb motoneurons of decerebrate cats. J. Neurophysiol. *80*, 2038–2045.

121. Huh, S., Heckman, C.J., and Manuel, M. (2021). Time Course of Alterations in Adult Spinal Motoneuron Properties in the SOD1(G93A) Mouse Model of ALS. eNeuro *8*.

122. Verneuil, J., Brocard, C., Trouplin, V., Villard, L., Peyronnet-Roux, J., and Brocard, F. (2020). The M-current works in tandem with the persistent sodium current to set the speed of locomotion. PLOS Biology *18*, e3000738.

## Supplemental Figures and Tables

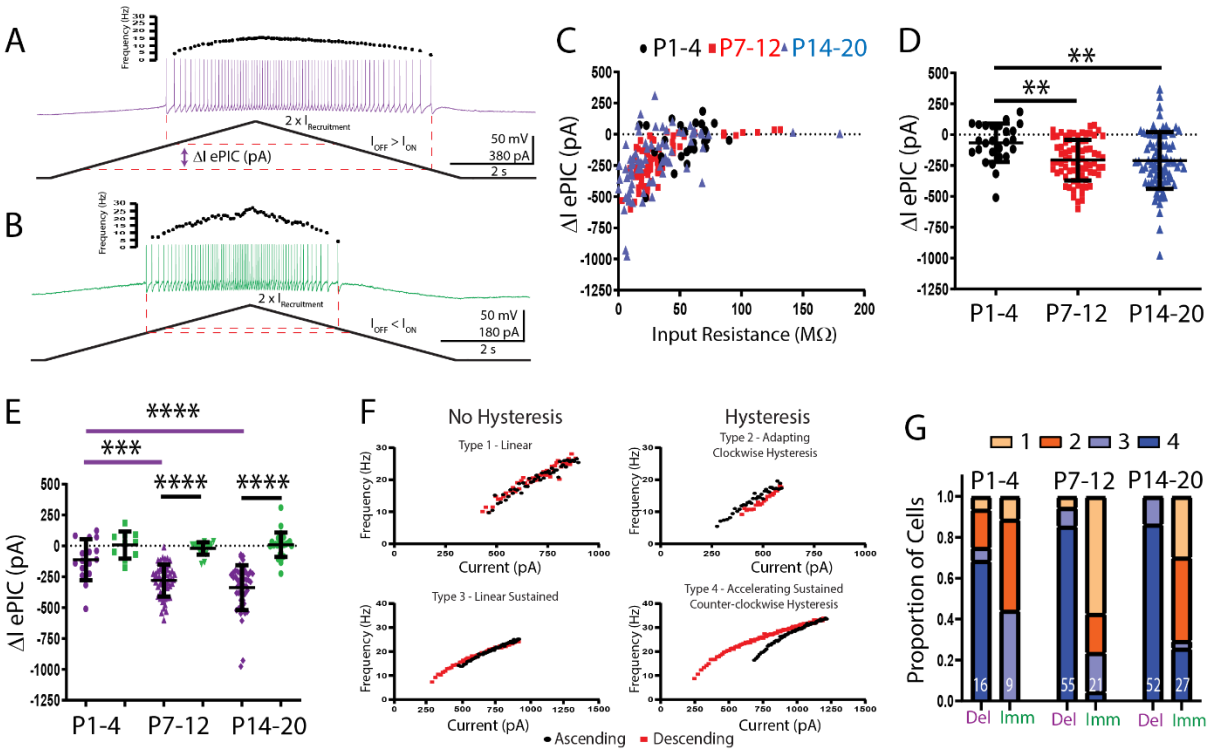


**Supplementary Figure 1: Maturation of recruitment-derecruitment and firing hysteresis during postnatal development.** Representative traces of the membrane potential and repetitive firing from a fast (A: purple) and slow (B: green) motoneuron during a triangular depolarizing current ramp up to an intensity of 2 x their respective recruitment currents. Recruitment-derecruitment hysteresis (ePIC), characterized by a lower current at derecruitment on the descending limb compared to recruitment on the ascending limb, producing a negative Delta I, is suggestive of the activation of a persistent inward current (PIC). Delta I is correlated with input resistance (C), increases after week 2 (D), but only in fast type motoneurons (E). Statistical analyses were conducted with one or 2-way ANOVA and Holm-Sidak post hoc analysis when significant effects were detected. Asterisks denote significant differences from Holm-Sidak post hoc analysis * $p < 0.05$, ** $p < 0.01$, *** $p < 0.001$, **** $p < 0.0001$. F.) Four patterns of firing rate hysteresis can be identified as described by Li and Bennett, 2006, with types 3 and 4 suggestive of PIC action. G.) Relative proportion of firing hysteresis types in fast and slow motoneurons across three weeks of postnatal development.

**Supplementary Table 1: Passive, recruitment, repetitive firing, and single spike properties of fast and slow motoneuron subtypes across three postnatal weeks.** Passive properties include whole cell capacitance, tau, input resistance and resting membrane potential (RMP). Recruitment properties: Recruitment current, derecruitment current, current firing range, voltage threshold of the first spike, and relative distance between RMP and spike threshold. Repetitive firing properties measured following recruitment on slow depolarizing current ramps include minimum firing rate, firing rate at 2 x recruitment current (RC) and maximum firing rate and the slope of the sub primary range (SPR). Single spike (action potential) properties including spike amplitude, rise time, and half width were measured from threshold, and afterhyperpolarization amplitude and half width, were elicited with a 10 ms square current pulse applied at 1.25 x rheobase. Statistics: Data were analyzed using 2 Factor ANOVA with MN type (Fast and Slow) and developmental week (Week 1, 2, 3) as factors. Statistical analyses addressed 3 core questions: 1.) Was there a difference between subtypes? 2.) Did it change during development? 3.) Do the subtypes mature differentially during development? Statistical results listing F and p values from 2 factor ANOVA addressing these questions are listed sequentially: 1: Main effect of subtype; 2: Main effect of development; 3: Subtype x development interaction. All data are presented as mean ± SD (min, max). P values are derived from Holm-Sidak post hoc comparisons within weeks, between MN types. Superscript numbers denote significant differences from Holm-Sidak within MN types, between weeks (1: week 1; 2: week 2; 3: week 3).

| **Postnatal Maturation of Fast and Slow Motoneuron Intrinsic Properties (257 cells from 95 animals)** | | | | | |
|---|---|---|---|---|---|
| **Parameter** | | **Week 1 (P1-4)[1]**<br>**54 cells, 18 animals** | **Week 2 (P7-12)[2]**<br>**122 cells, 42 animals** | **Week 3 (P14-20)[3]**<br>**81 cells, 35 animals** | **2W ANOVA F, p** |
| **Passive Properties** | | | | | |
| Capacitance (pF) | Fast | 285±94(112,542)[2,3] | 494±211(139,1191)[1] | 467±271(63,1220)[1] | 32.1, 3.9e-8<br>9.9, 6.8e-5<br>3.6, 0.03 |
| | Slow | 243±73(139,378) | 312±191(67,668) | 258±99(116,433) | |
| | P value | 0.9 | 3.6e-6 | 6.5e-6 | |
| Tau (ms) | Fast | 17.1±7.4(4.2,37.6)[3] | 13.5±5.0(3.4,27.7) | 9.9±5.7(2.1,34.4)[1] | 41.5,5.9e-10<br>1.1, 0.3<br>7.9, 4.7e-4 |
| | Slow | 17.8±7.9(6.8,35.7)[2,3] | 26.1±19.0(6.1,75.0)[1] | 25.6±19.6(3.7,82)[1] | |
| | P value | 0.97 | 1.8e-7 | 7.8e-8 | |
| Passive Input Resistance (MΩ) | Fast | 65.1±33.0(21.7,167.5)[2,3] | 30.8±15.9(10.4,114.1)[1] | 27.2±18.6(6.6,93.4)[1] | 78.9, >1.0e-15<br>0.7, 0.5<br>10.6, 3.9e-5 |
| | Slow | 76.6±35.5(30.4,114.1)[3] | 94.4±62.5(22.3,290.5) | 106.0±88.2(18.1,400)[1] | |
| | P value | 0.6 | 5.3x10e-12 | 1.2e-12 | |
| Steady State Input Resistance (MΩ) | Fast | 49.4±17.1(22.0,99.9)[2,3] | 27.2±18.4(2.8,99.4)[1] | 17.7±13.9(0.06,68)[1] | 52.9, 4.5e-12<br>3.7, 0.03<br>6.6, 0.002 |
| | Slow | 57.2±18.4(17.2,90.0) | 73.5±65.4(17.8,326.0) | 59.9±42.5(15.7,180) | |
| | P value | 0.6 | 1.4e-10 | 6.1x10^-7 | |
| Resting Membrane Potential (mV) | Fast | -62.6±4.0(-69.0,-50.0)[3] | -63.9±4.2(-72.0,-52.0)[3] | -66.8±3.6(-77,-60.0)[1,2] | 25.5, 8.4e-7<br>10.4, 4.4e-5<br>4.4, 0.01 |
| | Slow | -61.7±4.4(-69.0,-50.0)[2] | -58.3±5.4(-72.0,-52.0)[1,3] | -61.5±6.9(-73.0,-51.0)[2] | |
| | P value | 0.8 | 1.3e-8 | 3.5e-5 | |
| **Recruitment Properties (Ramp)** | | | | | |
| Recruitment Current (pA) | Fast | 349±214(118,1010)[2,3] | 550±254(149,1619)[1,3] | 816±631(127,2929)[1,2] | 45.4, 1.1e-10<br>3.4, 0.04<br>12.1, 9.6e-6 |
| | Slow | 327±178(101,757) | 235±225(23,891) | 173±176(23,797) | |
| | P value | 0.8 | 1.0e-4 | 2.3e-12 | |
| Derecruitment Current (pA) | Fast | 1038±300(286,1501)[2,3] | 2372±752(967,4605)[1,3] | 3624±1374(1586,7828)[1,2] | 27.1, 4.0e-7<br>57.1, >1.0e-15<br>14.1, 1.7e-6 |
| | Slow | 1290±344(413,1862)[3] | 1661±659(394,25430) | 2151±999(726,4023)[1] | |
| | P value | 0.99 | 0.001 | 1.7e-10 | |
| Current Firing Range (pA) | Fast | 937±297(210,1490)[2,3] | 1810±678(604,3776)[1,3] | 2853±1029(1136,6236)[1,2] | 24.7, 1.1e-6<br>70.1,>1.0e-15<br>3.4, 0.03 |
| | Slow | 695±251(154,1089)[2,3] | 1396±571(311,2379)[1,3] | 1962±965(699,3904)[1,2] | |
| | P value | 0.99 | 0.08 | 7.0e-6 | |
| First Spike TH (mV) | Fast | -37.9±3.7(-44.8,-29.0)[3] | -38.8±3.3(-45.2,-31.2)[3] | -43.7±3.8(-51.8,-34.4)[1,2] | 7.4, 0.007<br>80.4, >1.0e-15<br>6.6, 0.002 |
| | Slow | -36.6±3.1(-43.5,-30.2)[2,3] | -41.3±4.6(-51.2,-30.5)[1,3] | -47.2±4.5(-54.1,-35.7)[1,2] | |
| | P value | 0.4 | 0.02 | 5.3e-4 | |
| Spike TH-RMP (mV) | Fast | 24.5±5.4(11.3,22.9) | 24.2±4.8(10.2,23.8) | 26.5±5.3(17.6,25.9) | 35.6, 8.5e-9<br>5.7, 0.004 |
| | Slow | 25.1±5.6(12.3,19.8)[2,3] | 17.9±7.0(3.8,30.3)[1] | 18.9±7.1(6.3,30.5)[1] | |

| | | | | | |
|---|---|---|---|---|---|
| | P value | 0.9 | 1.0e-8 | 6.0e-7 | 9.7, 9.2e-5 |
| **Repetitive Firing Properties on Ramp** | | | | | |
| Minimum Firing Rate (Hz) | Fast | 10.9±3.7(6.9,24.0) [3] | 10.5±5.2(4.9,43.8) [3] | 6.9±2.2(4.5,15.2) [1,2] | 2.4, 0.1<br>15.1, 6.5e-7<br>6.7, 0.002 |
| | Slow | 11.3±4.8(6.2,24.3) [2,3] | 7.1±2.4(2.4,13.4) [1] | 7.4±2.5(2.2,12.3) | |
| | P value | 0.99 | 0.01 | 0.99 | |
| Firing Rate at 2x Recruitment Current (Hz) | Fast | 24.7±5.8(14.2,38.6) | 28.9±8.3(13.1,53.2) [3] | 24.5±9.8(8.2,52.6) [2] | 33.7, 2.0e-8<br>1.9, 0.2<br>3.0, 0.05 |
| | Slow | 21.2±5.3(13.3,38.5) | 17.9±9.6(3.4,45.3) | 17.1±12.8(5.4,61.4) | |
| | P value | 0.99 | 4.8e-8 | 0.009 | |
| Maximum Firing Rate (Hz) | Fast | 36.1±6.4(19.6,49.0) [2,3] | 45.6±9.4(27.5,83.3) [1] | 46.6±11.8(30.6,73.5) [1] | 7.3, 0.007<br>58.5, >1.0e-15<br>37.5, 7.0e-14 |
| | Slow | 28.3±6.7(16.9,39.7) [3] | 37.6±10.6(20.9,60.2) [3] | 82.4±45.2(25.4,196) [1,2] | |
| | P value | 0.99 | 0.4 | 7.0e-15 | |
| SPR FI slope (Hz/pA) | Fast | 0.084±0.03(0.03,0.15) | 0.096±0.06(0.01,0.41) [3] | 0.07±0.05(0.02,0.24) [2] | 0.3, 0.6<br>2.5, 0.08<br>12.2, 8.7e-6 |
| | Slow | 0.062±0.03(0.013,0.12) [3] | 0.065±0.02(0.03,0.11) [3] | 0.11±0.08(0.02,0.31) [1,2] | |
| | P value | 0.99 | 0.03 | 0.006 | |
| **Single Spike Properties** | | | | | |
| Amplitude (mV) | Fast | 75.5±4.3(66,84) | 73.0±5.3(60,87) | 74.8±6.8(61,89) | 6.5, 0.01<br>3.2, 0.04<br>2.0, 0.14 |
| | Slow | 75.2±5.9(61,87) | 76.2±7.8(62,92) | 76.7±10.4(68,91) | |
| | P value | 0.99 | 0.1 | 0.2 | |
| Spike rise time (ms) | Fast | 0.77±0.15(0.40,1.0) [2,3] | 0.59±0.12(0.31,0.92) [1,3] | 0.47±0.08(0.34,0.65) [1,2] | 39.3, 1.6e-9<br>85.9, >1.0e-15<br>7.1, 0.001 |
| | Slow | 0.98±0.28(0.40,1.49) [2,3] | 0.78±0.22(0.45,1.38) [1,3] | 0.50±0.18(0.28,1.2) [1,2] | |
| | P value | 2.6e-5 | 8.4x10e-8 | 0.8 | |
| Spike Half width (ms) | Fast | 0.99±0.22(0.53,1.39) [2,3] | 0.66±0.14(0.44,0.99) [1,3] | 0.57±0.11(0.38,0.82) [1,2] | 28.1, 2.5e-7<br>128, >1.0e-15<br>13.5, 2.7e-6 |
| | Slow | 1.26±0.28(0.73,1.95) [2,3] | 0.89±0.34(0.48,2.38) [1,2] | 0.51±0.13(0.32,0.81) [1,2] | |
| | P value | 5.8e-6 | 3.2e-7 | 0.2 | |
| AHP Amplitude (mV) | Fast | 6.7±2.2(3.6,12.7) | 6.6±2.0(2.9,12.3) | 6.3±2.5(1.3,12.5) | 0.07, 0.78<br>6.4, 0.002<br>9.3, 1.3e-4 |
| | Slow | 4.5. ±1.9(1.1,9.6) [2,3] | 7.3±2.5(2.5,11.9) [1] | 7.5±3.6(1.6,14.9) [1] | |
| | P value | 0.008 | 0.6 | 0.3 | |
| AHP Half width (ms) | Fast | 61.1±18.8(31.8,135.1) [2,3] | 43.3±12.7(22.1,80.1) [1] | 49.9±19.7(14.6,94.9) [1] | 38.8, 2.0e-9<br>1.1, 0.3<br>6.7, 0.001 |
| | Slow | 66.9±20.2(24.7,107.4) | 75.8±31.3(32.1,152.3) | 67.7±32.6(24.7,136.2) | |
| | P value | 0.6 | 4.0e-11 | 6.1 e-3 | |

**Supplementary Table 2: Active properties of fast and slow motoneurons subtypes across three postnatal weeks.** Characteristics of the subthreshold membrane potential trajectory during slow depolarizing recruitment current ramps. Presented are the acceleration onset voltage, acceleration amplitude, passive recruitment current estimated based on the initial linear trajectory of the membrane potential, actual measured recruitment current, and an estimate of the underlying persistent inward current (ePIC) that produces the membrane potential acceleration. Delta reflect the difference in derecruitment and recruitment currents on triangular depolarizing current ramps and provides an additional estimate of PIC. PICs were measured in voltage clamp during weeks 2-3 with the onset voltage, peak voltage, current amplitude, and densities measured. Sag conductance was estimated during weeks 1-3 and underlying h current (Ih) measured with amplitude and density at -70 mV and -110 mV presented. Time constant (tau) of Ih. Statistics: Data were analyzed using 2 Factor ANOVA with MN type (Fast and Slow) and developmental week (Week 1, 2, 3) as factors. Statistical analyses addressed 3 core questions: 1.) Was there a difference between subtypes? 2.) Did it change during development? 3.) Do the subtypes mature differentially during development? Statistical results listing F and p values from 2 factor ANOVA addressing these questions are listed sequentially: 1: Main effect of subtype; 2: Main effect of development; 3: Subtype x development interaction. All data are presented as mean ± SD (min, max). P values are derived from Holm-Sidak post hoc comparisons within weeks, between MN types. Superscript numbers denote significant differences from Holm-Sidak within MN types, between weeks (1: week 1; 2: week 2; 3: week 3).

| **Postnatal Maturation of Active Properties in Fast and Slow Motoneurons** | | | | | |
|---|---|---|---|---|---|
| **Parameter** | | **Week 1 (P1-4)[1]** | **Week 2 (P7-12)[2]** | **Week 3 (P14-20)[3]** | **2W ANOVA F, p** |
| **Subthreshold Membrane Potential Acceleration on Recruitment Ramp** | | | | | |
| Acceleration onset voltage (mV) | Fast | -49.1±3.8(-53.9, -39.8) [2,3] | -51.8±2.5(-57.2, -45.5) [1] | -51.4±4.4(-59.1, -35.9) [1] | 1.9, 0.2<br>24.9,1.4e-10<br>6.1, 0.003 |
| | Slow | -48.0±4.4(-56.5, -38.2) [2,3] | -52.0±3.4(-57.3,-44.2) [1,3] | -55.6±3.1(-57.8, -47.0) [1,2] | |
| | P value | 0.7 | 0.8 | 0.003 | |
| Acceleration Amplitude (dV) Spike TH – Acceleration onset (mV) | Fast | 11.0±3.7(4.4,21.3) | 12.9±2.3(7.0,18.5) | 12.1±3.4(6.1,24.9) | 4.1, 0.04<br>0.9, 0.4<br>2.2, 0.1 |
| | Slow | 11.6±4.2(3.8,20.6) | 11.0±4.1(3.8,22.2) | 10.5±3.4(3.4,17.6) | |
| | P value | 0.98 | 0.1 | 0.5 | |
| Passive Rec Current (pA) | Fast | 497±280(168,1267) [2,3] | 1017±492(268,2560) [1,3] | 1498±1100(272,4154) [1,2] | 66.7, 1.7e-13<br>7.1, 0.001<br>15.8, 3.4e-7 |
| | Slow | 433±218(115,985) | 411±392(57,1518) | 250±164(60,672) | |
| | P value | 0.9 | 6.8e-7 | 1.0e-15 | |
| Actual Rec Current (pA) | Fast | 349±214(118,1010) [2,3] | 550±254(149,1619) [1,3] | 816±631(127,2929) [1,2] | 45.4, 1.1e-10<br>3.4, 0.04<br>12.1, 9.6e-6 |
| | Slow | 327±178(101,757) | 235±225(23,891) | 173±176(23,797) | |
| | P value | 0.8 | 1.0e-4 | 2.3e-12 | |
| ePIC Passive-Actual Rec Current (pA) | Fast | 150±107(-18,439) [2,3] | 500±348(101,1855) [1,3] | 727±579(137,3072) [1,2] | 44.4, 1.8e-9<br>10.9, 3.0e-5<br>10.2, 5.6e-5 |
| | Slow | 116±105(-32,389) | 174±216(5.0,1110) | 112±110(23,519) | |
| | P value | 0.99 | 4.9e-5 | 6.4e-14 | |
| **Recruitment-derecruitment Hysteresis and Persistent Inward Current** | | | | | |
| Delta I Hysteresis (pA) | Fast | -112±165(-510,123) [2,3] | -280±129(-601, -10) [1,3] | -339±181(-976, -71) | 85.9, <1.0e-15<br>5.8, 0.004<br>6.1, 0.003 |
| | Slow | 7.7±110(-178,184) | -20±51(-147,37) | 9.2±99.3(309, -224) | |
| | P value | 0.2 | 7.1e-10 | 1.0e-16 | |
| PIC onset (mV) | Fast | | -50.2±4.1(-59.7, -39.9) | -49.0±4.6(-59.0, -42.5) | 57.6, 2.2e-10<br>0.3, 0.6<br>0.2, 0.7 |
| | Slow | | -58.3±4.4(-67.0, -51.5) | -58.2±4.9(-64.1, -49.1) | |
| | P value | | 5.0e-6 | 6.0e-6 | |
| PIC peak (mV) | Fast | | -32.8±5.0 (-45.7, -22.7) | -30.2±6.3(-37.6, -19.4) | 38.6, 5.1e-8<br>0.85, 0.4<br>1.3, 0.3 |
| | Slow | | -39.6±5.4(-53.3, -32.0) | -39.9±4.7(-53.1, -34.3) | |
| | P value | | 0.0032 | 0.0005 | |
| PIC amplitude (pA) | Fast | | 386±236(60, 1055) | 502±205(175,950) | 17.9, 7.8e-5<br>5.8, 0.02<br>0.02, 0.9 |
| | Slow | | 164±121 (52,366) | 271±80(49,680) | |
| | P value | | 0.007 | 0.03 | |
| PIC density (pA/pF) | Fast | | 0.87±0.45(0.17,1.95) [3] | 1.45±0.98(0.39,3.8) [2] | 5.3, 0.02<br>13.8, 4.4e-4<br>0.3, 0.6 |
| | Slow | | 0.60±0.35 (0.1, 1.3)[3] | 1.08±0.47(0.23,1.9) [2] | |
| | P value | | 0.3 | 0.2 | |
| **Sag and Ih** | | | | | |
| eSag Conductance (nS) | Fast | 3.6±3.5(-5.5,12.9) [3] | 6.5±13.1(-41.6,43.2)[3] | 31.9±35.9(-25.2,129.1) [1,2] | 7.5, 0.007<br>7.3, 8.3e-4<br>5.2, 0.006 |
| | Slow | 4.3±5.3(-2.2,25.2) | 6.0±15.8(-28.7,49.0) | 7.2±6.7(-2.6,28.7) | |
| | P value | 0.99 | 0.99 | 8.9e-7 | |

| | | | | | |
|---|---|---|---|---|---|
| Ih amplitude (-70 mV) (pA) | Fast | | -25±42(4.2, -113) [3] | -119±103(-7.3, -275) [2] | 14.4, 3.0e-4<br>5.3, 0.02<br>13.4, 5.3e-4 |
| | Slow | | -23±93(50.6, -116) | -1.9±14.4(23.1, -26.2) | |
| | P value | | 0.98 | 2.0e-5 | |
| Ih Density (-70 mV) (pA/pF) | Fast | | -0.05±0.1(0.2, -0.2) [3] | -0.53±0.85(-0.01, -3.0) [2] | 3.6, 0.06<br>2.5, 0.1<br>6.0, 0.02 |
| | Slow | | -0.12±0.1(0.15, -0.4) | -0.015±0.07(0.1, -0.1) | |
| | P value | | 0.99 | 0.01 | |
| Ih amplitude (-110 mV) (pA) | Fast | | -776±535(-67, -1472) [3] | -1176±557(-131, -2749) [2] | 29.5, 1.1e-6<br>1.3, 0.3<br>6.1, 0.02 |
| | Slow | | -449±330(-51, -902) | -302±196(-94, -640) | |
| | P value | | 0.009 | 3.0e-7 | |
| Ih Density (-110 mV) (pA/pF) | Fast | | -1.8±1.4(-0.25, -5.5) [3] | -4.6±5.8(-0.5, -21.4) [2] | 4.9, 0.03<br>2.0, 0.2<br>4.0, 0.05 |
| | Slow | | -1.6±1.0(-0.4, -3.4) | -1.2±0.76(-0.17, -2.6) | |
| | P value | | 0.99 | 0.015 | |
| Ih tau (-110 mV) (s) | Fast | | 0.37±0.11(0.3,0.7) [3] | 0.22±0.07(0.1,0.3) [2] | 50.1, 4.1e9<br>31.2, 1.0e-6<br>50.1, 4.1e-9 |
| | Slow | | 0.51±0.09(0.4,0.7) [3] | 0.41±0.05(0.3,0.5) [2] | |
| | P value | | 0.005 | 1.5e-9 | |